

# Turbulence spreading and anomalous diffusion on combs

Alexander V. Milovanov

*ENEA National Laboratory, Centro Ricerche Frascati, I-00044 Frascati, Rome, Italy and  
Max Planck Institute for the Physics of Complex Systems, 01187 Dresden, Germany*

Alexander Iomin

*Solid State Institute, Technion, Haifa, 32000, Israel and  
Max Planck Institute for the Physics of Complex Systems, 01187 Dresden, Germany*

Jens Juul Rasmussen

*Physics Department, Technical University of Denmark, DK-2800 Kgs. Lyngby, Denmark*

This paper presents a simple model for such processes as chaos spreading or turbulence spillover into stable regions. In this simple model the essential transport occurs via inelastic resonant interactions of waves on a lattice. The process is shown to result universally in a subdiffusive spreading of the wave field. The dispersion of this spreading process is found to depend exclusively on the type of the interaction process (three- or four-wave), but not on a particular instability behind. The asymptotic transport equations for field spreading are derived with the aid of a specific geometric construction in the form of a comb. The results can be summarized by stating that the asymptotic spreading pursues as a continuous-time random walk (CTRW) and corresponds to a kinetic description in terms of fractional-derivative equations. The fractional indexes pertaining to these equations are obtained exactly using the comb model. A special case of the above theory is a situation when two waves with oppositely directed wave vectors couple together to form a bound state with zero momentum. This situation is considered separately and associated with the self-organization of wave-like turbulence into banded flows or staircases. Overall, we find that turbulence spreading and staircasing could be described based on the same mathematical formalism, using the Hamiltonian of inelastic wave-wave interactions and a mapping procedure into the comb space. Theoretically, the comb approach is regarded as a substitute for a more common description based on quasilinear theory. Some implications of the present theory for the fusion plasma studies are discussed and a comparison with the available observational and numerical evidence is given.

## I. INTRODUCTION

Turbulence spreading [1] is the spillover into surrounding stable areas of turbulent motions excited at some location. The phenomenon characterizes both fluid and plasma turbulence and has been reported experimentally and/or numerically for a variety of systems and physical conditions, with a wealth of data spanning solar and astrophysics [2, 3], geophysics [4, 5] and magnetic confinement fusion [6–9]. In fusion grade plasmas, turbulence occurring in the linearly active (unstable) regions of a plasma can penetrate into the linearly inactive (stable) regions of the same plasma, where it can modify transport scalings [1, 6] and eventually deteriorate confinement [7–15]. More recently, it has been discussed [16–18] that turbulence spreading can mediate the global self-organization of L-mode tokamak plasma into a marginally stable state and that it underlies such phenomena as the rise and decay of transport barriers [18–21], scrape-off layer (SOL)-core and SOL-edge coupling [16, 22], avalanche transport [23–26], and the staircase self-organization [27–36]. Indirect evidence of turbulence spreading may be obtained from, e.g., the breakdown of gyro-Bohm transport scaling [16, 37], the breakdown of Fick’s law [16, 38], the broadening of SOL [39, 40], and the transport shortfall problem [17, 18, 22]. Further evidence comes along with cold-pulse phenomenology [41]

and the observations of internal rotation reversal [41, 42] and pulse-polarity reversal [42–44], yet among other observations [8, 16].

On the theory side, a brief account of the existing literature suggests the absence of a unifying theory of turbulence spreading that would apply in all cases. One popular approach [1, 6, 10–16] assumes a diffusion-reaction dynamics with sources and sinks, leading to a kinetic description in terms of the Fisher-Kolmogorov-Petrovsky-Piskunov (F-KPP) equation [45–47] and its modifications. By mastering a suitable nonlinearity in the diffusion coefficient and in respective driving and damping terms one succeeds based on this equation to reproduce a number of transport situations of interest to fusion tasks (e.g., Refs. [8, 18, 26]) under certain rather weak conditions. A criticism raised against this approach, however, is that it relies on a phenomenological characterization of turbulence spreading and uses a Gaussian propagator of turbulence intensity, which is not at all obvious in nonequilibrium systems. Other approaches [48–51] advocate an idea that turbulence spreading can be understood as a transport problem for fluctuation pulses, suggesting a theoretical description in terms of Burgers’ equation with noise. In the context of tokamak plasma, the Burgers’ model can be formulated [16, 51] so that it includes both inward spreading from SOL into edge and outward spreading from edge into SOL. In the latter case it mim-

ics turbulence overshoot by coherent structures, vortices and blob-filaments [52–55]. In the outer core–inner edge region, the observed phenomenology [7, 42, 56] of turbulence spreading is captured by the Hasegawa-Wakatani model [57–59] of plasma edge turbulence, revealing a spatially anisotropic transport with bursts [60–64].

In the realm of wave turbulence [65, 66]—composed of a large number of interacting waves with a distribution of frequencies and wave vectors—the problem of turbulence spreading can be reconciled [67] with the fundamental problem of quantum localization of dynamical chaos [68]. The latter problem has been extensively studied and discussed in the literature in the framework of the nonlinear Schrödinger equation with random potential (e.g., Refs. [69–78]). In that context, a spillover into stable regions occurs because the overlap between the components of a nonlinear field induces internal pressure that squeezes the wave function into the ambient space despite the inhomogeneities present. The phenomenon leads universally to an unlimited subdiffusive spreading of the wave field under the action of a weak (Ginzburg-Landau style) nonlinearity [69, 70, 76]. The authors of Refs. [74, 76] have suggested that the dynamics of this spreading process can be understood based on continuous-time random walks (CTRWs), leading to a theoretical description in terms of fractional-derivative equations [79–81].

By CTRW—a statistical model introduced in physics by Montroll and Weiss [82, 83]—one means a random-walk process with a distribution of either step-sizes (Gaussian or Lévy [84]) or waiting times between steps (Poisson or fat-tailed) or both. As such, CTRWs underpin nondiffusive generalizations [79, 80, 85] of the Brownian random walk [85, 86], thus opening up the doorway to outstanding applications in such areas as, for instance, disordered solid materials [87, 88], dielectric relaxation [88, 89], and magnetic confinement fusion [90–93].

In this study, we build upon these ideas and devise a theory of turbulence spreading based on the Hamiltonian of inelastic wave-wave interactions on a lattice. In this fashion, we relate the transport problem for turbulence intensity to a first-principal description of nonlinear wave-wave couplings. In particular, we show, following Ref. [67], that the spreading dynamics depends exclusively on whether the interaction process is three- or four-wave-like, regardless of the specific instability behind. We then obtain the fractional kinetic equations for asymptotic spreading by employing a topological mapping procedure onto the Dirac comb.

In mathematics, a Dirac comb (e.g., Ref. [94]) is a geometric approximation of the pulse function

$$\mathcal{C}_\Lambda(x) := \sum_{m=-\infty}^{+\infty} \delta(x - m\Lambda), \quad (1)$$

where  $\Lambda$  is the period of the comb (period between consecutive pulses),  $m = 0, \pm 1, \pm 2, \dots$  is an integer counter, and  $\delta(x)$  denotes the Dirac delta-function.

A Dirac comb (see Fig. 1) consists of a central back-

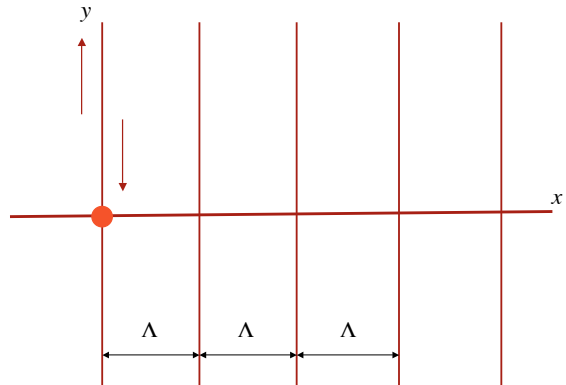


FIG. 1: The Dirac comb. The central horizontal line is the backbone, the vertical lines are the side branches, or “fingers” of the comb. The bright red circle on the left is the origin.  $\Lambda$  is the spacing between neighboring side branches,  $x$  is the coordinate along the backbone, and  $y$  is the coordinate in fingers.

bone along the  $x$  axis and infinite side branches (fingers or teeth) in the  $y$  direction. Note that the number of side branches is countable (because the set of all integer numbers is countable).

From a dynamical perspective, combs and their generalizations provide a convenient geometric representation of CTRWs (because side branches can operate as dynamical traps with a distribution of exit times). On the other hand, because combs are loopless structures (similarly to Bethe lattices [94]), their transport properties can in many situations be determined exactly [95–97].

The appreciation of combs in physics began with the work of Ziman [98], who introduced them as a simplification of the percolation model of de Gennes [99]. In Ziman’s description, a percolation cluster is thought of as composed of a conducting path, which corresponds to the backbone, and side branches, which represent the dead-ends of the cluster. Then at some level of idealization one draws a connected graph with infinite teeth that resembles a comb. Such comb-like graphs as in Fig. 1 have been applied in a basic theory of CTRWs as an alternative to fractal lattices (Refs. [94, 97, 100]).

A remarkable feature about combs is that they capture much of the actually observed signatures of anomalous transport in disordered systems (e.g., Refs. [94, 101, 102]). In fusion grade plasmas, the use of combs is less noted, with only few exceptions, among which we specifically mention a model of the plasma staircase [103] and a demonstration, supported by numerical evidence, of weak localization of plasma avalanches [104].

The paper is organized as follows. The asymptotic scaling laws for turbulence spreading are derived first (Secs. II A and II B), followed by a derivation of the exit-

time distributions in Sec. II C. These derivations suggest a special case of the zero-frequency resonance, which is considered separately in Sec. III. The comb model is formulated in Sec. IV. Section V introduces the basic transport model and its 1D reduction, the partial cases of which are analyzed in Sec. VI. Next, the fractional relaxation equation is discussed (Sec. VII). We summarize our findings in Sec. VIII. Some auxiliary results pertaining to the comb model are presented in Appendix A.

## II. GENERAL CASE

We envisage turbulence as a superposition of a large number of interacting waves with the dispersion relation  $\omega_{\mathbf{k}_i} = \omega_i(\mathbf{k}_i)$ , where  $\omega_{\mathbf{k}_i}$  is the frequency of the  $i$ th wave, and  $\mathbf{k}_i$  is the wave vector. The conservation of energy and momentum through the interaction process implies that the interaction cross-section has sharp peak whenever there is a resonance among the waves involved and vanishes otherwise. Respectively for three- and four-wave interactions the conditions for a resonance read [65]

$$\omega_{\mathbf{k}} = \omega_{\mathbf{k}_1} + \omega_{\mathbf{k}_2}, \quad \mathbf{k} = \mathbf{k}_1 + \mathbf{k}_2, \quad (2)$$

and

$$\omega_{\mathbf{k}_1} + \omega_{\mathbf{k}_2} = \omega_{\mathbf{k}_3} + \omega_{\mathbf{k}_4}, \quad \mathbf{k}_1 + \mathbf{k}_2 = \mathbf{k}_3 + \mathbf{k}_4, \quad (3)$$

$$\omega_{\mathbf{k}_1} = \omega_{\mathbf{k}_2} + \omega_{\mathbf{k}_3} + \omega_{\mathbf{k}_4}, \quad \mathbf{k}_1 = \mathbf{k}_2 + \mathbf{k}_3 + \mathbf{k}_4. \quad (4)$$

The triad equations (2) [and similarly the quartic Eqs. (3) and (4)] may be thought of as defining equations for the wave vectors  $\mathbf{k}_i$ . These equations might or might not have a solution in general as the dispersion relation  $\omega_{\mathbf{k}_i} = \omega_i(\mathbf{k}_i)$  imposes a nontrivial constraint on admissible frequencies and wave vectors. If a solution exists, it may be of three types. One type is associated with parametric decay instability, i.e., a process when strong falling wave decays into two or more lower-frequency waves such as in Figs. 2 and 3, top. This process is thresholded in that the falling wave's amplitude must exceed a certain critical level for the actual breakup to occur. Another type is exact opposite process when two or more waves merge into one stronger wave. Finally, and this is specific to four-wave interactions, two falling waves may participate in an inelastic scattering process such as in Fig. 3, bottom, in which process the energy and momentum are merely redistributed among the participating waves, while the number of waves is preserved. These decay, merger and scattering processes are all important in far-from-equilibrium plasma systems, particularly in scenarios underlying the expansion of turbulence into surrounding stable areas (e.g., Refs. [11, 12, 67]).

In this paper's work, we are interested in the expansion of a small puff of turbulence excited locally by some process (for instance, by injecting a strong pump wave into a plasma [66]). The injected power is assumed to be

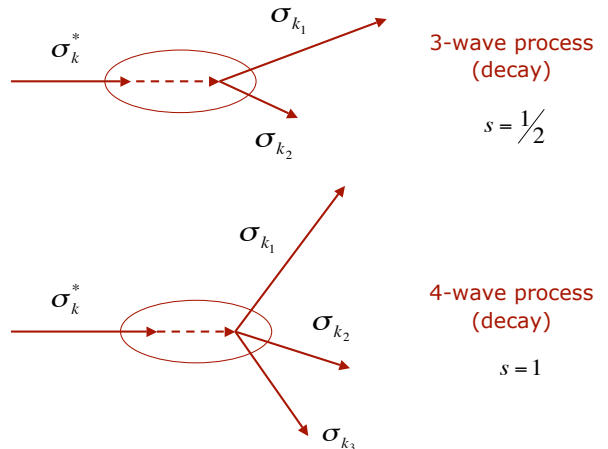


FIG. 2: Resonant decay processes. Top: A three-wave decay process when a falling wave breaks into two offspring waves. Bottom: The analogue four-wave process when a falling wave breaks into three offspring waves.  $\sigma_k$  and other sigmas alike denote complex amplitudes of the various processes involved and are explained in the main text [see the paragraph after Eq. (6)]. The  $s$  index pertains to Eqs. (23) and (35). The oval (and the dashed line inside) both stand to remind that the interaction processes above refer to waves, not particles, meaning these processes might *not* be spatially localized.

sufficient to trigger a cascade of secondary decay events, whether three- or four-wave, or both, thus populating the system with some initial number of unstable modes. Once locally excited, the instability can propagate to large spatial scales when nonlinearity, such as a spatial pressure inhomogeneity [59, 60], couples different waves, and energy and momentum conservation conditions are met at each step of the nonlinear interaction process.

In fusion applications, one encounters a situation according to which noninteracting waves can propagate freely along a preferred direction (usually it is the poloidal direction in a tokamak), while being linearly localized in the perpendicular (radial) direction. In tokamak geometry, a running wave must meet the known constraints [59, 105] imposed by poloidal and toroidal periodicities, through which periodicities the noninteracting waves are stuck to rational magnetic flux surfaces. When nonlinear interactions are allowed, then the main effect these interactions have on the wave field is to induce instability on neighboring flux surfaces, which is equivalent to an expansion of the wave field in the direction of radial localization. It is this process of instability expansion driven by nonlinear interactions which we associate with the phenomenon of turbulence spreading. The implication is that the spreading process (in its wave formulation) can be fundamentally *anisotropic*—it may occur in a direction perpendicular to wave vectors  $\mathbf{k}_i$  (perpendicular to the preferred direction), while the interactions propagate along the  $\mathbf{k}_i$ 's. This situation is

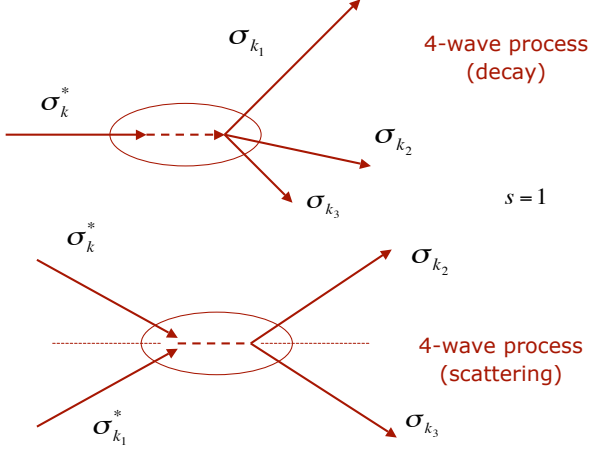


FIG. 3: A four-wave decay (top) versus scattering (bottom) process: a schematic illustration. Same notation as in Fig. 2 above.

somewhat different from an (apparently similar) nonlinear Anderson problem [69, 70, 76], where the squeezing occurs in the direction of the  $\mathbf{k}$  vector (in one dimension).

In this study, we approximate the phenomena of turbulence spreading with a 1D interaction model as follows. It is assumed that all interactions occur on a 1D regular lattice, which is aligned with the direction of wave propagation. The spreading is in perpendicular (radial) direction and comes about as a result of nonlinear interaction among the different unstable modes along the lattice, provided the necessary conditions of energy and momentum conservation [Eqs. (2)–(4)] are satisfied. We argue it is the fundamental structure of these interactions, which is key to understand and predict the resulting asymptotic transport scalings.

With these implications in mind, we abandon hereafter the vector notation in Eqs. (2)–(4), and continue with a scalar description instead. In particular, we use  $k$  instead of  $\mathbf{k}$ , which is defined as the scalar product  $k = \mathbf{k} \cdot \hat{\mathbf{e}}$ , where  $\hat{\mathbf{e}}$  is a unit vector in the preferred direction. Note that  $k$  may have either sign depending on whether  $\mathbf{k}$  goes along or against the  $\hat{\mathbf{e}}$  vector. Yet so, we refer to  $k$  as “wave vector” for simplicity. A reflection symmetry  $\mathbf{k} \longleftrightarrow -\mathbf{k}$  is assumed, i.e., the 1D lattice on which the interactions occur is isotropic. With this last convention, the dispersion relation is simplified to  $\omega_{k_i} = \omega_i(|k_i|)$ , implying  $\omega_{k_i} = \omega_{-k_i}$ .

### A. Three-wave interactions

The Hamiltonian of three-wave interactions on a discrete lattice reads (e.g., Refs. [65, 106])

$$H = H_0 + H_{\text{int}}, \quad H_0 = \frac{1}{2} \sum_k \omega_k \sigma_k^* \sigma_k, \quad (5)$$

$$H_{\text{int}} = \frac{1}{3} \sum_{k, k_1, k_2} V_{-k, k_1, k_2} \sigma_k^* \sigma_{k_1} \sigma_{k_2} \delta_{-k+k_1+k_2, 0}, \quad (6)$$

where  $H_0$  is the Hamiltonian of noninteracting waves,  $H_{\text{int}}$  is the interaction Hamiltonian,  $\sigma_k = \sigma_k(t)$  are complex amplitudes which represent a wave process with frequency  $\omega_k$  and wave vector  $k$  and which may depend on time  $t$  in general,  $\omega_{-k} = \omega_k$  thanks to  $\omega_k = \omega(|k|)$ ,  $\sigma_{-k} = \sigma_k^*$  by way of temporal translation symmetry [65], the asterisk denotes complex conjugate, the set of all  $k$ 's is countable (in a discrete model),  $V_{-k, k_1, k_2}$  are complex coefficients which characterize the cross-section of an interaction process with triad couplings  $k = k_1 + k_2$ , and  $\delta_{-k+k_1+k_2, 0}$  is the Kronecker delta, which accounts for resonant character of these interactions. Remembering that the lattice is isotropic, i.e.,  $\omega_k = \omega(|k|)$  for all  $k$ , the summation in Eq. (5) is performed over both positive and negative values of  $k$  allowed by the dispersion relation. For the same reason, the summation in Eq. (6) goes over all positive and negative values of  $k, k_1, k_2$  allowed jointly by the dispersion relation  $\omega_{k_i} = \omega_i(|k_i|)$  and conservation laws. This, together with the sign-reversal conditions  $\sigma_{-k} = \sigma_k^*$  for all  $k$  and  $V_{-k, k_1, k_2} = V_{k, -k_1, -k_2}^*$  for all  $k, k_1$ , and  $k_2$ , guarantees that the Hamiltonian in Eqs. (5) and (6) is real and well-defined. The cubic terms  $\sigma_k^* \sigma_{k_1} \sigma_{k_2}$  in Eq. (6) incorporate all admissible three-wave interaction processes, of both the decay type and the merger type, in which processes  $\sigma_k^*$  represents the falling wave, and  $\sigma_{k_1}$  and  $\sigma_{k_2}$  represent the offspring waves (see Fig. 2, top).

Given the Hamiltonian in Eqs. (5) and (6), one applies the canonical equations

$$\dot{\sigma}_k = i \frac{\partial H}{\partial \sigma_k^*}, \quad \dot{\sigma}_k^* = -i \frac{\partial H}{\partial \sigma_k} \quad (7)$$

to obtain the equations of motion for the complex amplitudes  $\sigma_k$ , i.e.,

$$\dot{\sigma}_k = i\omega_k \sigma_k + iV^* \sigma_{k_1} \sigma_{k_2}. \quad (8)$$

The equations for  $\sigma_{k_1}$  and  $\sigma_{k_2}$  are obtained either directly from the Hamiltonian  $H = H_0 + H_{\text{int}}$  by applying the canonical equations, or by switching indexes in the equations of motion (8) on account of the resonance condition  $k = k_1 + k_2$  and the general rule  $\sigma_{-k} = \sigma_k^*$ . The end result is

$$\dot{\sigma}_{k_1} = i\omega_{k_1} \sigma_{k_1} - iV \sigma_k \sigma_{k_2}^*, \quad (9)$$

$$\dot{\sigma}_{k_2} = i\omega_{k_2} \sigma_{k_2} - iV \sigma_k \sigma_{k_1}^*. \quad (10)$$

In the above,  $V \equiv V_{k, -k_1, -k_2}$  for simplicity, and the upper dot denotes time differentiation.

If the field is spread across  $\Delta n \gg 1$  states (in radial direction), then the conservation of the total probability

$$\sum_{n=0}^{\Delta n} |\sigma_n|^2 \simeq \int_0^{\Delta n} |\sigma_n|^2 dn = 1 \quad (11)$$

implies that the density of the probability is small and is inversely proportional to  $\Delta n$ , i.e.,  $|\sigma_n|^2 \simeq 1/\Delta n$ .

It is understood that the evolution of the wave field in time is due to nonlinear coupling among the resonant modes. The rate of excitation of a newly involved mode is obtained as intensity of this coupling process, i.e.,  $R \simeq \rho|V^*|^2|\sigma_{n_1}\sigma_{n_2}|^2$ , where  $\rho$  is a coefficient. Using dynamical Eqs. (8)–(10), one gets

$$R \simeq \rho|V|^2|\sigma_n|^4 \simeq \rho|V|^2/(\Delta n)^2, \quad (12)$$

where the scaling  $|\sigma_n|^2 \simeq 1/\Delta n$  has been considered. In writing Eq. (12) we have tacitly assumed that the number of modes in Eqs. (8)–(10) is large enough to render  $\Delta n \gg 1$ . The latter condition guarantees that  $R \ll \omega_k$  for the majority of modes, i.e., radial expansion is slow compared to a typical wave frequency. Said differently, the spreading process is quasistatic, enabling  $\sigma_{-k} = \sigma_k^*$  whenever needed. On the other hand, the resonant character of interactions dictates

$$R = d\Delta n/dt, \quad (13)$$

which is a reincarnation of Fermi's golden rule (e.g., Ref. [107]) known from quantum mechanics. Combining Eqs. (12) and (13), one obtains

$$d\Delta n/dt = \rho|V|^2/(\Delta n)^2. \quad (14)$$

Integrating over time in Eq. (14), one is led to  $(\Delta n)^3 = 3\rho|V|^2 t$ , yielding

$$(\Delta n)^2 = (3\rho)^{2/3}|V|^{4/3}t^{2/3}. \quad (15)$$

One sees that the asymptotic spreading is subdiffusive:  $(\Delta n)^2$  grows slower-than-linear with time as  $t \rightarrow +\infty$ .

In the context of fusion plasma, one usually looks into a spatial spread  $\Delta x$  instead of the number of states,  $\Delta n$ . However, if the linear field is spatially localized in radial direction, and if the localization mechanism is such as described by Garbet *et al.* [1] (i.e., stickiness to rational flux surfaces), then  $\Delta n$  is just proportional to radial spread, i.e.,  $\Delta n \propto \Delta x$ . From Eq. (15) one infers  $\Delta x \propto t^{1/3}$ . This is remarkable, as the latter scaling coincides with the scaling [6, 10] deduced from the F-KPP equation.

## B. Four-wave interactions

In the case of four-wave interactions (see Fig. 3), the interaction Hamiltonian becomes

$$H_{\text{int}} = \frac{1}{4} \sum_{k, k_1, k_2, k_3} V_{-k, k_1, k_2, k_3} \sigma_k^* \sigma_{k_1} \sigma_{k_2} \sigma_{k_3} \delta_{-k+k_1+k_2+k_3, 0} \quad (16)$$

and represents a next-order correction to the three-wave interaction Hamiltonian introduced in Sec. II A. As usual [65], temporal translation symmetry dictates  $\sigma_{-k} = \sigma_k^*$  for all  $k$  and  $V_{-k, k_1, k_2, k_3} = V_{k, -k_1, -k_2, -k_3}^*$  for all  $k, k_1,$

$k_2$ , and  $k_3$ . It is assumed that the dispersion relation  $\omega_{k_i} = \omega_i(k_i)$  is symmetric with respect to the inversion  $k_i \rightarrow -k_i$ , i.e.,  $\omega_{k_i} = \omega_i(|k_i|)$ , where  $k_i = \mathbf{k}_i \cdot \hat{\mathbf{e}}$ . The summation in Eq. (16) is performed over all admissible values of  $k, k_1, k_2, k_3$  allowed by the dispersion relation  $\omega_{k_i} = \omega_i(|k_i|)$  and conservation laws, that is, any  $k_i$  is included on an equal footing with  $-k_i$ , where  $k_i = k, k_1, k_2, k_3$ . This guarantees that  $H_{\text{int}}$  is real and well-defined. By replacing  $k \rightarrow k_{i_1}$ ,  $k_1 \rightarrow -k_{i_2}$ ,  $k_2 \rightarrow k_{i_3}$ , and  $k_3 \rightarrow k_{i_4}$ , and making use of  $\sigma_{-k_{i_2}} = \sigma_{k_{i_2}}^*$ , one rewrites  $H_{\text{int}}$  in an equivalent “symmetric” form, i.e.,

$$H_{\text{int}} = \frac{1}{4} \sum_{k_{i_1} + k_{i_2} = k_{i_3} + k_{i_4}} V_{-k_{i_1}, -k_{i_2}, k_{i_3}, k_{i_4}} \sigma_{k_{i_1}}^* \sigma_{k_{i_2}}^* \sigma_{k_{i_3}} \sigma_{k_{i_4}}. \quad (17)$$

In the above, the quartic terms  $\sigma_{k_{i_1}}^* \sigma_{k_{i_2}}^* \sigma_{k_{i_3}} \sigma_{k_{i_4}}$  represent complex amplitudes of individual four-wave interaction events (scatterings, decays and mergers all count), the asterisk marks the falling waves, and we have omitted the Kronecker delta  $\delta_{-k_{i_1} - k_{i_2} + k_{i_3} + k_{i_4}, 0}$  for simplicity.

The fact that  $H_{\text{int}}$  collects both scatterings and decays via  $\omega_{k_i} = \omega_i(|k_i|)$  has important physics implications. Indeed, it is shown theoretically [108] and confirmed numerically [109] that a certain amount of decays taking place is actually necessary in order for inelastic scatterings to occur. When the scatterings couple an increased number of waves (meaning nonlinearity exceeds a certain critical level), the system of interacting waves obeying Eqs. (3)–(4) naturally (without tuning of parameters) transits into a stochastic state, in which state it develops statistical, rather than deterministic, properties. It is this transition into a stochastic state that underlies the occurrence of “turbulence” in large systems of interacting modes. In what follows, it is tacitly assumed that the necessary conditions [109] for the stochastic instability to come into play have been satisfied, thus paving the way for the random dynamics [65, 110], and to a theoretical description in terms of the probability density function (Secs. V and VI).

If one wants to single out the effect of four-wave interactions on the dynamics of field spreading (or if three-wave interactions are forbidden by the dispersion relation), then the procedure is to substitute (16) into Eq. (5) (in place of the three-wave  $H_{\text{int}}$ ) and apply the canonical equations (7), from which the following equations of motion for the complex amplitudes  $\sigma_k$  may be deduced:

$$\dot{\sigma}_k = i\omega_k \sigma_k + iV^* \sigma_{k_1} \sigma_{k_2} \sigma_{k_3}, \quad (18)$$

where we have denoted  $V \equiv V_{k, -k_1, -k_2, -k_3}$  and  $V^* \equiv V_{-k, k_1, k_2, k_3}$ . Switching the indexes in Eq. (18) and remembering that  $\sigma_{-k} = \sigma_k^*$ , one gets the dynamical equations for  $\sigma_{k_1}$ , i.e.,

$$\dot{\sigma}_{k_1} = i\omega_{k_1} \sigma_{k_1} - iV \sigma_k \sigma_{k_2}^* \sigma_{k_3}^*, \quad (19)$$

and similarly for  $\sigma_{k_2}$  and  $\sigma_{k_3}$ . The rate of field spreading is obtained as  $R \simeq \rho|V^*|^2|\sigma_{n_1}\sigma_{n_2}\sigma_{n_3}|^2$ , leading to [cf.

Eq. (12)]

$$R \simeq \rho |V|^2 |\sigma_n|^6 \simeq \rho |V|^2 / (\Delta n)^3, \quad (20)$$

where  $\rho$  is a coefficient,  $|\sigma_n|^2 \simeq 1/\Delta n$  in conformity with the conservation law in Eq. (11), and we have assumed that  $\Delta n$  is as large as to guarantee  $R \ll \omega_k$  for the majority of  $k$ 's. Combining Eq. (20) with Fermi's golden rule  $R = d\Delta n/dt$ , one gets

$$d\Delta n/dt = \rho |V|^2 / (\Delta n)^3, \quad (21)$$

from which  $(\Delta n)^4 = 4\rho |V|^2 t$ . The latter equation corresponds to a subdiffusive spreading for  $t \rightarrow +\infty$ , i.e.,

$$(\Delta n)^2 = (4\rho)^{1/2} |V| t^{1/2}. \quad (22)$$

The subdiffusive scaling law in Eq. (22) is a familiar one. Indeed this scaling law is actually known from quantum chaotic dynamics, where it characterizes the spreading of a quantum wave packet in nonlinear Schrödinger lattices with disorder [75, 111–114]. This correspondence with quantum chaos is no surprise as we have based our model on Fermi's golden rule [Eq. (13)], with that justification that the interactions are resonant. If, instead of the golden rule, we applied the random-phase approximation as of Refs. [69, 76, 77], then a different scaling law would have emerged for  $t \rightarrow +\infty$ , i.e.,  $(\Delta n)^2 \propto t^{2/5}$ . We disregard this scaling law here.

### C. Exit-time distribution

The subdiffusive scaling laws in Eqs. (15) and (22) correspond to a non-Markovian spreading process with exit-time statistics. The demonstration uses the idea of clustering of unstable modes in phase space (Refs. [74, 112]). Mathematically, it is convenient to unify the spreading laws in Eqs. (14) and (21) by defining

$$d\Delta n/dt = A / (\Delta n)^{2s+1}, \quad (23)$$

where the switcher  $s$  takes the value  $s = 1$  for four-wave interactions and the value  $s = 1/2$  for three-wave interactions, and we have denoted  $A = \rho |V|^2$  for simplicity. Integrating over time in Eq. (23), one gets  $(\Delta n)^{2s+2} = (2s+2)At$ , from which

$$(\Delta n)^2 = [(2s+2)A]^{1/(s+1)} t^{1/(s+1)}. \quad (24)$$

Differentiating both sides of Eq. (23) with respect to time and eliminating the resulting  $d\Delta n/dt$  on the right-hand side with the aid of the same Eq. (23), one obtains

$$\frac{d^2}{dt^2} \Delta n = -\frac{(2s+1)A^2}{(\Delta n)^{4s+3}}. \quad (25)$$

Finally, by rewriting the power-law function on the right-hand side such that it takes the form of a gradient against  $\Delta n$ , one gets

$$\frac{d^2}{dt^2} \Delta n = -\frac{d}{d\Delta n} \left[ -\frac{A^2/2}{(\Delta n)^{4s+2}} \right]. \quad (26)$$

Equation (26) is equivalent to the Newton equation of motion of a point particle of unit mass in the potential field

$$W(\Delta n) = -\frac{A^2/2}{(\Delta n)^{4s+2}}, \quad (27)$$

where  $\Delta n$  has the sense of position coordinate and characterizes the actual span of the field distribution.

If  $s = 1$ , then the potential function in Eq. (27) becomes

$$W(\Delta n) = -\frac{A^2/2}{(\Delta n)^6}. \quad (28)$$

The latter potential is known from molecular physics, where it quantifies the attractive interactions between atoms inside molecules (as a constituent of the Lennard-Jones potential [115]). Given this insight and the fact that the potential function in Eq. (27) has attractive character for any  $s > 0$ , one might arguably propose that the newly excited modes form clusters, or “molecules” in phase space [74, 112], where they will be effectively trapped [113] due to their nonlinear coupling.

Multiplying both sides of Eq. (26) by the velocity  $d\Delta n/dt$  and integrating the ensuing differential equation with respect to time, after a simple algebra one obtains

$$\frac{1}{2} \left[ \frac{d}{dt} \Delta n \right]^2 - \frac{A^2/2}{(\Delta n)^{4s+2}} = \Delta E, \quad (29)$$

where the first term on the left-hand side has the sense of kinetic energy of a particle, and the second term is its potential energy.

More so, it is shown using Eq. (23) that the kinetic energy in Eq. (29) compensates for the potential energy *exactly*, that is, the full energy in Eq. (29) is zero, i.e.,  $\Delta E = 0$ . Furthermore, both the negative potential energy  $W(\Delta n) = -A^2/2(\Delta n)^{4s+2}$  and the positive kinetic energy  $\frac{1}{2}(d\Delta n/dt)^2 = A^2/2(\Delta n)^{2(2s+1)}$  vanish while spreading. Both will decay as the  $(4s+2)$ th power of the number of states and the ratio between them will *not* depend on width of the field distribution.

The full energy being equal to zero implies that a particle with the equation of motion (26) is sitting on the separatrix  $\Delta E = 0$ . That means that the motion process of this particle may be particularly sensitive to perturbations [110, 116, 117]. Such perturbations may have different physics origins—from thermal noise to imprecision in the initial conditions [110]—though the main cause is arguably the neglect of higher-order interaction terms in an idealized three- or four-wave picture of interactions [118]. Here, we assume, following Refs. [67, 112], that the role of random factors can be accounted for using the energy parameter  $T$ , and we interpret this as the “temperature” of thermal bath enveloping the separatrix.

Adding thermal fluctuations to the Lennard-Jones model in Eq. (27) leads directly to a non-Poissonian distribution of exit times with the divergent mean, as we now proceed to show.



In fact, the probability for a given mode to quit the cluster after it has traveled  $\Delta n$  sites on it is given by the Boltzmann factor

$$p(\Delta n) = \exp[W(\Delta n)/T], \quad (30)$$

where  $W(\Delta n)$  is the negative potential energy stemming from the equation of motion (26). Substituting  $W(\Delta n)$  from Eq. (27), one writes

$$p(\Delta n) = \exp[-A^2/2T(\Delta n)^{4s+2}]. \quad (31)$$

Taylor expanding the exponential function for  $\Delta n \gg 1$ , one gets

$$p(\Delta n) \simeq 1 - A^2/2T(\Delta n)^{4s+2}. \quad (32)$$

The probability to remain (survive) on the cluster after  $\Delta n$  space steps is  $p'(\Delta n) = 1 - p(\Delta n)$ , yielding

$$p'(\Delta n) \simeq A^2/2T(\Delta n)^{4s+2}. \quad (33)$$

Eliminating  $\Delta n$  with the aid of Eq. (24), one obtains the probability to survive on the cluster after  $\Delta t$  time steps

$$p'(\Delta t) \propto (\Delta t)^{-(2s+1)/(s+1)}, \quad (34)$$

which is equivalent to an exit-time distribution

$$\chi_\alpha(\Delta t) \propto (\Delta t)^{-(1+\alpha)} \quad (35)$$

with  $\alpha = s/(s+1) < 1$ . Specifically, one finds  $\alpha = 1/3$  for three-wave interactions ( $s = 1/2$ ) and  $\alpha = 1/2$  for four-wave interactions ( $s = 1$ ). One sees that the integral

$$\int_{\sim 1}^{\tau} \Delta t \chi_\alpha(\Delta t) d\Delta t \sim \int_{\sim 1}^{\tau} (\Delta t)^{-\alpha} d\Delta t \sim \tau^{1-\alpha} \rightarrow +\infty \quad (36)$$

diverges for  $\tau \rightarrow +\infty$ , implying that the mean exit time is infinite for all  $\alpha < 1$ .

### III. SPECIAL CASE

A special case of the above theory is a situation when two waves with oppositely directed wave vectors  $k_j$  and  $-k_j$  couple together to form a bound state with zero momentum. The process is similar to the generation of the Cooper pairs in superconductors [119]. An interesting regime occurs when such states can participate in triad interactions with high  $\mathbf{k}$  running ways by way of the zero-frequency resonance (see a schematic illustration in Fig. 4, top)

$$\omega_{k_i} = \omega_0 + \omega_{k_i-0}, \quad (37)$$

where  $k_i$  and  $k_i - 0$  denote the wave vectors of the running wave just before and after the interaction event, and  $\omega_0 \rightarrow 0$  is the frequency of the bound state. A situation of the kind is found in tokamaks, where the three-wave resonance in Eq. (37) is held responsible for

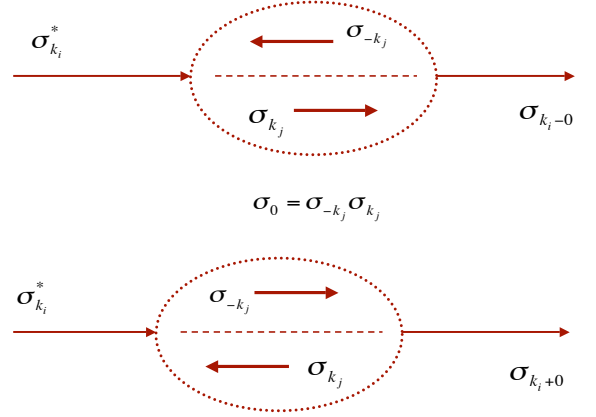


FIG. 4: The zero-frequency resonance. The oval structure (dotted line) represents a bound state between two counter-propagating waves with complex amplitudes  $\sigma_{-k_j}$  and  $\sigma_{k_j}$ . Top: A running wave transfers energy to a bound state via the zero-frequency resonance. Bottom: A bound state transferring energy to the running wave.

the generation of zonal flows [21, 120, 121]. By zonal flows one means azimuthally symmetric band-like shear flows, which are ubiquitous phenomena in planetary atmospheres, oceans and the laboratory [4, 21, 27, 122]. In the context of tokamak plasma, zonal flows are zero-frequency electrostatic potential fluctuations with finite radial wave number. These zonal flows are driven exclusively by nonlinear interactions, which transfer energy from electrostatic micro-turbulence into large-scale drift-like motion of plasma particles with electrostatic  $\mathbf{E} \times \mathbf{B}$  drift. Usually, such nonlinear interactions are three-wave triad couplings between two high  $\mathbf{k}$  drift waves and one low  $\mathbf{k}$  zonal flow excitation [21]. The importance of zonal flows in magnetic confinement fusion is that these flows help to reduce the levels of turbulence and turbulent transport by absorbing the free energy from the high  $\mathbf{k}$  turbulent background.

The coupling process in Eq. (37) corresponds to the interaction Hamiltonian

$$H'_{\text{int}} = \sum_{k_i > 0} V_{-k_i, 0, k_i-0} \sigma_{k_i}^* \sigma_0 \sigma_{k_i-0} \delta_{-k_i+0+k_i-0, 0}, \quad (38)$$

where  $\sigma_0$  is the amplitude of a bound state with frequency  $\omega_0 \rightarrow 0$ , the summation goes over all positive values of  $k_i$  allowed by the dispersion relation, and we have kept the Kronecker delta for consistency with previous equations.

The Hamiltonian in Eq. (38) is joined by the Hamiltonian of exact opposite process

$$H''_{\text{int}} = \sum_{k_i > 0} V_{-k_i, -0, k_i+0} \sigma_{k_i}^* \sigma_0^* \sigma_{k_i+0} \delta_{-k_i-0+k_i+0, 0}, \quad (39)$$

which characterizes the decay of a bound state with frequency  $\omega_0 \rightarrow 0$  via the zero-frequency resonance  $\omega_{k_i} = -\omega_0 + \omega_{k_i+0}$  (see Fig. 4, bottom).

There is a subtlety here, however, and this refers specifically to fine structure of the bound states. Indeed, if the frequency of the bound states is about zero, i.e.,  $\omega_0 \rightarrow 0$ , and if these states are formed by two counter-propagating waves having vanishing frequency each, then the resonance condition in Eq. (37) can be satisfied [123] if only for the bound state as a whole as well as for each of the partial wave processes involved composing this state. This is because the resonance in Eq. (37) has finite width, which allows for a margin on admissible resonant frequencies. This finite spread over frequencies gives rise to an instability of the bound state—akin to stochastic instability of coupled nonlinear oscillators [110, 116]—which occurs along the separatrix  $\omega_0 = 0$ . The latter is a hypersphere in wave number space, with the center at zero wave number vector  $\mathbf{k} = 0$  and of radius  $|\mathbf{k}_j|$  (see Sec. 7 of Ref. [124]).

More explicitly, if the interaction frequency  $\omega_0 \rightarrow 0$ , then the distance between resonances in vicinity of the separatrix behaves as  $\delta\omega \sim \omega_0$ , while the nonlinear resonance width [65] approaches zero in accordance with  $\Delta\omega_{\text{NL}} \propto \sqrt{\omega_0}$  [67] and for  $\omega_0 \rightarrow 0$  will be much greater than  $\delta\omega$ , i.e.,  $\Delta\omega_{\text{NL}} \propto \sqrt{\omega_0} \gg \delta\omega \sim \omega_0$ . The implication is that the zero-frequency resonance in Eq. (37) is broad enough to cover the constituent wave processes across the bound state. This zero-frequency instability, which is generic to isotropic systems with separatrix dynamics [65, 117], has been simulated numerically in Ref. [124] in the context of surface waves in a fluid.

Writing the amplitude of the bound state as  $\sigma_0 = \sigma_{-k_j}\sigma_{k_j}$ , where  $\sigma_{-k_j}$  and  $\sigma_{k_j}$  are complex amplitudes of the constituent wave processes, and substituting into Eq. (38), one may represent the interaction Hamiltonian  $H'_{\text{int}}$  in an equivalent four-wave form

$$H'_{\text{int}} = \sum_{k_i > 0, k_j > 0} V_{-k_i, -k_j, k_j, k_i} \sigma_{k_i}^* \sigma_{k_j}^* \sigma_{k_j} \sigma_{k_i} \delta_{-k_i - k_j + k_j + k_i, 0}, \quad (40)$$

where use has been made of  $\sigma_{-k_j} = \sigma_{k_j}^*$ . This Hamiltonian is a partial case of the “symmetric” Hamiltonian (17), with that particularity that the summation in Eq. (40) goes over positive values of  $k_i$  and  $k_j$ .

One sees that the zero-frequency resonance is special in that it can be considered as either a three- or four-wave interaction process depending on whether the zero-frequency state  $\sigma_0 = \sigma_{-k_j}\sigma_{k_j}$  is accounted for as one single wave with zero momentum or just as two coupled waves with oppositely directed momenta. This duality has important implications with regard to statistical characteristics of the resulting spreading process.

In fact, if one wants to assess the asymptotic ( $t \rightarrow +\infty$ ) dispersion of the wave field, then one needs to consider that the actual spreading rate  $R = d\Delta n/dt$  is limited to the generation of new bound states by way of the zero-frequency resonance in Eq. (37). In that regard, the zero-frequency state  $\sigma_0$  weighs as one single wave, suggesting the interaction Hamiltonian in Eq. (38) applies. The ensuing spreading law is obtained from Eq. (24), where one

demands  $s = 1/2$ , leading to

$$(\Delta n)^2 \propto t^{2/3}. \quad (41)$$

On the other hand, focusing on exit-time statistics, one turns back on three-wave interactions and starts looking into four-wave processes instead, with that justification that it is this type of interaction process that limits the lifetime of the bound states (and therefore is most relevant for an exit-time distribution). It is at this point where the four-wave interaction Hamiltonian in Eq. (40) comes into play. In this approximation, the fact that  $\sigma_0$  has internal structure is key, meaning the zero-frequency wave  $\sigma_0 = \sigma_{-k_j}\sigma_{k_j}$  weighs as much as two interacting waves. It is understood that four-wave interactions result in a steeper distribution of exit times [see Eq. (35)] and as such will have an upper hand in determining the decay instability of the bound states. With this implication in mind, the distribution of exit times is inferred from Eq. (35) by letting  $s = 1$  in  $\alpha = s/(s+1)$ , yielding

$$\chi_\alpha(\Delta t) \propto (\Delta t)^{-3/2}. \quad (42)$$

Summarizing the above reasoning, it is noted that the presence of zero-frequency states results in a mixed statistics, when the asymptotic spreading law is three-wave-like, while the distribution of exit times is four-wave-like.

In the context of tokamak plasmas, the spreading law in Eq. (41) can describe the radial expansion of drift-wave turbulence by way of coupling to zonal flows. The subdiffusive character of Eq. (41) suggests zonal flows may effectively suppress the radial transport. Indeed the fusion experiments demonstrate and direct computer simulations confirm that zonal flows can limit considerably the losses of hot thermonuclear plasma into the edge region (e.g., Refs. [9, 15, 120, 121, 125]; Refs. [21, 126] for reviews). This positive view should, however, be balanced by the fact that zonal flows simultaneously regenerate the turbulence through the decay process in Eq. (39).

An exciting result in the study of zonal flows in recent years has arguably been the discovery of quasiregular patterns of  $\mathbf{E} \times \mathbf{B}$  flows dubbed the  $\mathbf{E} \times \mathbf{B}$  staircase (or plasma staircase) [27–30]. Staircases are ubiquitous meso-scale dynamical structures characterized by narrow regions of localized gradient sharpening and of strong and lasting jets interspersed with broader regions of turbulent (typically, avalanching) transport (see Fig. 1 of Ref. [104]). Experimentally,  $\mathbf{E} \times \mathbf{B}$  staircases are identified in a large variety of plasma parameters in ion drift-wave turbulence using correlation analysis of high-resolution fast-sweeping reflectometry (e.g., Ref. [28]).

The plasma staircase exemplifies how a systematic organization of turbulent fluctuations may lead to the onset of strongly correlated flows on magnetic flux surfaces. Theoretically, the plasma staircase represents a synergetic cooperation between the transport by avalanches at the meso-scales and the spontaneously occurring zonal flows [16, 17]. The latter constitute a permeable localized barrier to avalanche propagation [127, 128].



Focusing on the interaction Hamiltonian in Eq. (40), one associates the zero-frequency states  $\sigma_0 = \sigma_{-k_j} \sigma_{k_j}$  with the different staircase jet zonal flows, where each such flow is labeled by a proper value of  $k_j$ . As each  $k_j$  is excited on its own resonant magnetic flux surface, the interaction Hamiltonian (40) with the sum over  $k_j$  predicts a quiregular (grid-like) pattern, as is indeed observed in the experiment [28, 29]. Developing these viewpoints, one might arguably propose that zonal flows naturally (through the overlap condition  $\Delta\omega_{NL} \gg \omega_0$ ) organize themselves into a quiregular, complex spatio-temporal pattern that one witnesses in the experiment as the  $\mathbf{E} \times \mathbf{B}$  staircase. In that regard, the subdiffusive scaling law in Eq. (41) represents the radial dispersion of electrostatic drift waves that would result if the staircase structure contained an infinite number of jets.

#### IV. THE COMB MODEL

Perhaps the most important observation from the above analysis is the absence of a characteristic temporal scale of the spreading process. The unstable modes are trapped within disconnected clusters of states by the action of the Lennard-Jones potential in Eq. (27), and whether they do or do not quit the clusters is statistical, with a broad distribution of exit times. In this paradigm, a meaningful spreading occurs when the new modes are excited outside the existing clusters. Self-similarity implies that new excitations happen on a probabilistic basis and that the statistical distribution of waiting times pertaining to these excitations is actually the same as the exit-time distribution in Eq. (35).

In this Section, we analyze the expansion of turbulent field as a transport problem in comb geometry. The main idea here is that one can map the subdiffusive scaling laws in Eqs. (15) and (22) onto a Dirac comb, and by doing so unveil the microscopic organization of the asymptotic spreading process. Technically, it is convenient to generalize the Dirac comb first, and to introduce a *comb space* by building the side branches *everywhere densely* along the backbone—instead of rising them at a fixed space step  $\Lambda$  (see a schematic illustration in Fig. 5). For instance, the side branches could be placed at all rational numbers along the  $x$  axis (because the rational numbers are everywhere dense in the set of real numbers). Because, on the other hand, the positive rational numbers can be made in one-to-one correspondence with the set of natural numbers [129], a comb space with dense side branches is equivalent to (has the same cardinality [130] as) the discrete comb in Eq. (1). That means that a comb space with everywhere dense in the backbone side branches contains the same infinite number of dynamical traps as the discrete comb does. It is understood that the asymptotic ( $t \rightarrow +\infty$ ) dispersion law is imposed by statistical distribution of waiting times spent within each such trap, and that all these traps are just identical copies of each other, suggesting one might rely

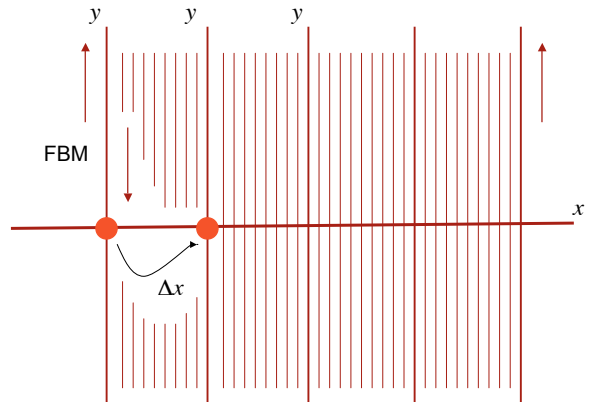


FIG. 5: The comb model. Side branches are shown as vertical lines and are assumed to be everywhere dense in the backbone (the horizontal line). The red circles represent the initial (left) and final (right) positions of the random walker performing a jump of the length  $\Delta x$  along the backbone (marked by the coordinate  $x$ ). Vertical arrows in the  $y$  direction represent the fractional Brownian motion (FBM) in side branches.

on either model to assess asymptotic dispersion. That said, a comb structure with dense side branches can be preferable to a discrete one as it simplifies the analysis behind the derivation of continuum equations (Sec. V). In the context of fusion plasma, the issue of dense side branches helps to account for the common properties of propagation of electrostatic drift waves that are attracted to rational flux surfaces [1, 21, 59]. At the same time, the observed equivalence between the two formulations (discrete versus dense) can result in a more direct association of combs with the zonal flows and staircases (Sec. VID). The comb model is formulated as follows.

Consider a comb structure with everywhere dense in the backbone side branches as in Fig. 5. At time  $t = 0$ , a motion process is initiated along an arbitrarily chosen side branch starting from an initial position on the backbone. This starting position, which is marked as  $(x = 0, y = 0)$ , is then used to set up a coordinate system in the entire comb space. In particular, we define  $x$  and  $y$  to be the position coordinates along the backbone and in side branches, respectively. The initial velocity is along  $y$ , if up- or downward, unimportantly.

Further concerning the motion process, we take it to be fractional Brownian motion, or FBM. By FBM—dating back to Mandelbrot and van Ness [131]—one means a Gaussian motion process such that the density of the probability to find a particle (random walker) at time  $t$  at the distance  $y$  away from the starting position is given by

$$f(y, t) = (4\pi K_\beta t^\beta)^{-1/2} \exp[-y^2/(4K_\beta t^\beta)], \quad (43)$$

where  $0 < \beta \leq 2$  is the exponent of FBM. The behavior

of FBM is antipersistent for  $0 < \beta < 1$  and persistent for  $1 < \beta \leq 2$  [132]. If  $\beta = 1$ , then FBM reduces to normal diffusion, which is neither persistent nor antipersistent. Often the exponent of FBM is written as  $\beta = 2H$ , where  $H$  is the Hurst exponent known from the time-series analyses [132, 133]. Using  $H$ , one writes the mean-squared displacement along  $y$  as

$$\langle (\Delta y)^2(t) \rangle \propto t^{2H}, \quad (44)$$

which is obtained straightforwardly as the second moment of the probability density function in Eq. (43).

Focusing on tokamak applications, we associate the actual  $H$  value with a competition between regular convection by the  $\mathbf{E} \times \mathbf{B}$  drift and the trapping effect due to electrostatic micro-turbulence within the  $\mathbf{E} \times \mathbf{B}$  flow. In this respect, the regular (convective) part favors long-time persistent behavior, with  $1/2 < H \leq 1$ , while the microscopic turbulence part imposes anti-persistent dynamics, characterized by  $0 < H < 1/2$ . The results, presented below, indicate  $H \leq 1/2$  (i.e., the turbulent part dominates).

Setting  $y = 0$  in Eq. (43), one obtains the probability to return to the starting position after  $\Delta t$  time steps, i.e.,

$$p_{y=0}(\Delta t) \propto (\Delta t)^{-H}, \quad (45)$$

where the relation  $H = \beta/2$  has been used. In particular, if  $H = 1/2$ , then  $p_{y=0}(\Delta t) \propto (\Delta t)^{-1/2}$ .

Next turning to the backbone transport, our assumptions are as follows. Any time the FBM walker returns to the backbone at  $y = 0$ , it either jumps to another side branch some  $\Delta x$  spatial steps away (with the probability  $q$ ), or remains with the current side branch (with the probability  $1 - q$ ). If the walker does change the branch on which it is currently sitting, then it restarts from the same position  $y = 0$  on the new side branch, and the process repeats itself. These settings are illustrated schematically in Fig. 5. We shall assume for simplicity, without losing in generality, that the probabilities to jump and to remain are both equal to  $q = 1 - q = 1/2$ , so the choice is random. Also we assume equal probabilities to jump along or against the  $x$  axis, that is, there is no bias along the backbone. Finally, we define that the probability density to choose a new side branch as far away as  $\Delta x$  spatial steps decreases with the number of steps as

$$p_\mu(\Delta x) \sim A_\mu |\Delta x|^{-(1+\mu)}. \quad (46)$$

That is,  $p_\mu(\Delta x)$  is a decaying power-law function of  $|\Delta x|$ . In the above,  $\mu$  is the exponent of the power law,  $A_\mu$  is a normalization parameter, and we have tacitly assumed that the jump lengths may span over a broad range of spatial scales. The implication is that the jumps need not occur between the neighboring side branches only (in the discrete formulation), but there is a wide choice instead, though with a decaying probability density to jump onto a more distant side branch. Concerning the  $\mu$  value, we restrict ourselves to the interval  $1 < \mu < 2$ . With this

setting, the power-law distribution in Eq. (46) is Lévy-stable for large jumps [84, 85]. The case  $0 < \mu < 1$ , though mathematically similar, is not considered here. Yet so, we include the limiting case  $\mu = 2$ , which is understood as Gaussian, or normal, distribution of the jump lengths (because the normal distribution is the upper bound on Lévy-stable laws for  $\mu \rightarrow 2$ ). Denoting the variance of the normal distribution as  $\lambda^2$ , we define

$$\lim_{\mu \rightarrow 2} p_\mu(\Delta x) = \exp(-|\Delta x|^2/2\lambda^2). \quad (47)$$

Remark that the normal distribution in Eq. (47) induces a characteristic jump length  $\Delta x \sim \lambda$  in the  $x$  direction. This contrasts the Lévy statistical case, with  $1 < \mu < 2$ , in which case the distribution of the jump lengths is scale free. As is well-known [79, 85, 134], the Lévy-stable distribution with  $1 < \mu < 2$  generates Lévy flights.

The comb model described above is a generalization to Lévy statistics of the random-walk model considered previously by Weiss and Havlin in Ref. [97]. In their model, the motion process in side branches is taken to be normal diffusion, not FBM. Also Weiss and Havlin assume a characteristic jump length along the backbone, which is matched by a regular spacing between the neighboring teeth. In our notation, Weiss and Havlin's model is reproduced for  $H = 1/2$ ,  $\beta = 1$ , and  $\mu = 2$ , leading to a waiting-time distribution  $\chi_\alpha(\Delta t) \propto (\Delta t)^{-3/2}$ . The analysis, presented below, suggests Weiss and Havlin's comb can characterize the spreading dynamics driven by four-wave interactions. Yet, their model fails to include if only triad interactions in Eq. (6) as well as the zero-frequency resonance in Eq. (37), in which cases one needs to introduce a Lévy-stable motion along the backbone, with a power-law distribution of the jump lengths in Eq. (46).

## V. TRANSPORT EQUATIONS

The asymptotic ( $t \rightarrow +\infty$ ) transport model for the random walk in comb geometry is obtained by coupling together the Gaussian diffusion equation [131, 132] for FBM in side branches with the space-fractional kinetic equation [79, 81, 134] for Lévy flights in the  $x$  direction. Because, by the assumptions made, a Lévy flight along  $x$  may only occur when FBM crosses the backbone at  $y = 0$ , we can write

$$\frac{\partial}{\partial t} f(x, y, t) = \left[ K_\beta t^{\beta-1} \frac{\partial^2}{\partial y^2} + \delta(y) K_\mu \frac{\partial^\mu}{\partial |x|^\mu} \right] f(x, y, t). \quad (48)$$

Here,  $f = f(x, y, t)$  is the probability density to find the random walker at time  $t$  at point  $(x, y)$  in the comb space,  $\delta(y)$  is the Dirac delta-function,  $K_\beta$  and  $K_\mu$  are coefficients of the transport process,

$$\frac{\partial^\mu}{\partial |x|^\mu} f(x, y, t) = \frac{1}{\Gamma_\mu} \frac{\partial^2}{\partial x^2} \int_{-\infty}^{+\infty} \frac{f(x', y, t)}{|x - x'|^{\mu-1}} dx' \quad (49)$$

is the Riesz fractional derivative [135, 136] of order  $\mu$ ,  $1 < \mu < 2$  is the fractal dimension of the Lévy flight,

and  $\Gamma_\mu = -2\cos(\pi\mu/2)\Gamma(2-\mu)$  is a normalization parameter. The latter parameter ensures smooth crossover to  $\partial^2/\partial x^2$  of the fractional operator  $\partial^\mu/\partial|x|^\mu$  as  $\mu \rightarrow 2$ , i.e.,  $\lim_{\mu \rightarrow 2} \partial^\mu/\partial|x|^\mu = \partial^2/\partial x^2$ . Note that the Riesz fractional derivative  $\partial^\mu/\partial|x|^\mu$  is an integro-differential operator for all  $0 < \mu < 2$  (in contrast to conventional derivatives of integer order). As such, it incorporates some non-locality of spreading dynamics (because the probability densities at points  $x$  and  $x'$  appear to be power-law correlated, with a fat-tailed two-point correlation function  $\propto 1/|x-x'|^{\mu-1}$ ). For  $\mu \rightarrow 2$ , the nonlocal features vanish by way of  $\partial^\mu/\partial|x|^\mu \rightarrow \partial^2/\partial x^2$ , giving rise to a local (in the sense of the central limit theorem [84]) asymptotic transport process. If  $\mu \rightarrow 1$ , then the Riesz fractional derivative (49) reduces to [137]

$$\frac{\partial^\mu}{\partial|x|^\mu} f(x, y, t) \rightarrow -\frac{1}{\pi} \frac{\partial}{\partial x} \int_{-\infty}^{+\infty} \frac{f(x', y, t)}{x-x'} dx', \quad (50)$$

where the spatial derivative  $\partial/\partial x$  is applied to the Hilbert transform operator. The latter operator is defined by [81]

$$\hat{\mathbf{H}}[f(x, y, t)] = \frac{1}{\pi} \int_{-\infty}^{+\infty} \frac{f(x', y, t)}{x-x'} dx'. \quad (51)$$

For  $\mu \rightarrow 2$ , the Lévy-fractional Eq. (48) becomes

$$\frac{\partial}{\partial t} f(x, y, t) = \left[ K_\beta t^{\beta-1} \frac{\partial^2}{\partial y^2} + \delta(y) K_2 \frac{\partial^2}{\partial x^2} \right] f(x, y, t), \quad (52)$$

where  $K_2$  characterizes diffusivity along the backbone. Letting  $\beta = 1$ , one obtains the Fokker-Planck equation in the comb space

$$\frac{\partial}{\partial t} f(x, y, t) = \left[ K_1 \frac{\partial^2}{\partial y^2} + \delta(y) K_2 \frac{\partial^2}{\partial x^2} \right] f(x, y, t), \quad (53)$$

which does not contain the scaling factor  $\sim t^{\beta-1}$  in front of the  $\partial^2/\partial y^2$  term.

We note in passing that the transport model in Eq. (53) with normal diffusion in side branches was considered by Arkhincheev and Baskin [138] as a model of subdiffusive transport along Weiss and Havlin's comb [97].

Note, also, that we write continuum equations for the probability density function  $f = f(x, y, t)$ , where  $x$  is a real number. This is licit as we rise side branches everywhere densely along the backbone, meaning any position  $x$  on the backbone can be approximated, as accurately as one likes, by a proper rational value [130].

A common feature among Eqs. (48), (52) and (53) is the presence of singularity in the backbone term  $\sim \delta(y) K_\mu \partial^\mu/\partial|x|^\mu$ . This singularity is represented by the Dirac delta-function,  $\delta(y)$ , and accounts for coupling between the transport processes along the backbone and in side branches. If  $y \neq 0$ , i.e., the random walker is outside the backbone, then the backbone term is cancelled out to zero, leaving back the familiar diffusion equation for FBM in the  $y$  direction, i.e.,

$$\frac{\partial}{\partial t} f(y, t) = K_\beta t^{\beta-1} \frac{\partial^2}{\partial y^2} f(y, t). \quad (54)$$

Based on this equation, one recovers the probability density in Eq. (43), from which the asymptotic dispersion law [132, 133] for FBM can be inferred, i.e.,

$$\langle (\Delta y)^2(t) \rangle = \int_{-\infty}^{+\infty} (\Delta y)^2 f(\Delta y, t) d\Delta y \propto t^\beta, \quad (55)$$

where  $\beta = 2H$  is the exponent of FBM, and  $t \rightarrow +\infty$ .

If  $y = 0$ , then instead of cancellation to zero one encounters a divergent behavior in the backbone term due to the Dirac delta-pulse. Technically, this is a problem, since the pulse function is non-analytical. To circumvent this difficulty, one may consider that the probability to return to the starting point in Eq. (45) is equivalent to a waiting-time distribution between consecutive steps of the random walk along the backbone, i.e.,

$$\chi_H(\Delta t) \sim dp_{y=0}(\Delta t)/d\Delta t \propto (\Delta t)^{-(H+1)}. \quad (56)$$

On account of this distribution one may write, instead of Eq. (48), the effective 1D equation

$$\frac{\partial}{\partial t} f(x, t) = {}_0D_t^{1-\beta/2} K_{\beta,\mu} \frac{\partial^\mu}{\partial|x|^\mu} f(x, t), \quad (57)$$

where

$${}_0D_t^{1-\beta/2} f(x, t) = \frac{1}{\Gamma(\beta/2)} \frac{\partial}{\partial t} \int_0^t \frac{f(x, t')}{(t-t')^{1-\beta/2}} dt' \quad (58)$$

is the Riemann-Liouville fractional derivative [135, 136] of the order  $1 - \beta/2 = 1 - H$ . Indeed, it is shown [79, 80] in a basic theory of CTRWs that the non-Poissonian distribution of waiting times in Eq. (56) leads directly to a time-fractional equation (57) with the Riemann-Liouville derivative (58) on the right-hand side. This fractional derivative of the order  $1 - H$  is a consequence of the fact that the mean waiting time resulting from (56) is infinite, i.e.,

$$\int_{\sim 1}^{\tau} \Delta t \chi_H(\Delta t) d\Delta t \propto \tau^{1-H} \rightarrow +\infty, \quad (59)$$

where  $\tau \rightarrow +\infty$ , and  $0 < H < 1$ .

We should stress that the model (57) is not really an equivalent of the original 2D model in Eq. (48), but is an effective 1D reduction of this [139], making it possible to avoid dealing with the singularity in the backbone term. This is achieved on the expense of introducing a special form of time differentiation using the Riemann-Liouville fractional operator (58). Mathematically, the Riemann-Liouville derivative (58) is analogous to the Riesz derivative in Eq. (49), though it uses a proper range of integration, with the lower limit set to  $t = 0$ . This lower limit is dictated by a condition that the walk process starts at the time  $t = 0$ . This way, the Riemann-Liouville operator incorporates the initial-value problem into the transport model. Remark that the transport equation (57) can be rewritten in an equivalent form using the Caputo fractional derivative [79, 135]—in that case the fractional

differentiation over time goes to the left-hand side of the corresponding transport equation (where it replaces the  $\partial/\partial t$  derivative), and has the order of fractional differentiation being equal to  $H = \beta/2$ . Because of this integro-differential character of fractional differentiation, the ensuing transport model proves to be non-Markovian, i.e., the current state of the transport process depends on the past states, with a long-time memory kernel.

Using kinetic Eq. (57), one obtains the fractional moments

$$\langle |\Delta x|^\gamma(t) \rangle \propto t^{\gamma\beta/2\mu} \quad (60)$$

of the  $f = f(x, t)$  distribution, from which the scaling of the pseudo mean-squared displacement  $\langle (\Delta x)^2(t) \rangle$  versus time can be deduced for  $t \rightarrow +\infty$ , i.e.,

$$\langle (\Delta x)^2(t) \rangle \equiv [\langle |\Delta x|^\gamma(t) \rangle]^{2/\gamma} \propto t^{\beta/\mu}, \quad (61)$$

where  $0 < \gamma < \mu \leq 2$ . In the above  $\langle \dots \rangle$  denotes the ensemble average, i.e.,  $\langle [\dots] \rangle = \int_{-\infty}^{+\infty} [\dots] dx$ , where the integration is performed in infinite limits along the backbone. Note that we obtain the pseudo mean-squared displacement in Eq. (61) by rescaling the fractional moment  $\langle |\Delta x|^\gamma(t) \rangle$  as the direct calculation of the second moment of  $f(x, t)$  yields a divergent result owing to the nonlocality of Lévy flights [79, 134].

Combining Eqs. (55) and (61), one obtains a relationship between the respective dispersions in the  $x$  and  $y$  directions, i.e.,

$$\langle (\Delta x)^2(t) \rangle \propto [\langle (\Delta y)^2(t) \rangle]^{1/\mu}. \quad (62)$$

This last equation shows that the diffusion on combs is inherently anisotropic, with a faster component along the side branches, and a slower component along the backbone (for  $1 < \mu \leq 2$ ).

## VI. TRANSPORT EQUATIONS CONTINUED

The fractional transport model in Eq. (57) characterizes the expansion of wave turbulence by inelastic wave-wave interactions for  $t \rightarrow +\infty$ . The actual dispersion law in physical space is obtained by identifying the backbone coordinate  $x$  with the radial spread  $\Delta x$ . The latter is proportional to the number of states  $\Delta n$  for the reasons explained in the end of Sec. II A, i.e.,  $\Delta x \propto \Delta n$ . We have, with the aid of Eq. (61),

$$\langle (\Delta n)^2(t) \rangle \propto t^{\beta/\mu}, \quad (63)$$

where we have kept angle brackets to emphasize that the scaling in Eq. (63) derives statistically by taking moments of the probability density function.

In what follows, we consider separately the three- and four-wave interaction cases, as well as the special case of the zero-frequency resonance:

### A. Three-wave interactions

In a three-wave process, the turbulence expansion law is given by the subdiffusive transport scaling in Eq. (15). By matching (15) to (63) one demands  $\beta/\mu = 2/3$ . The  $\beta$  value is obtained by comparing the waiting-time distributions in Eqs. (35) and (56), from which  $\alpha = H$ , yielding  $\beta = 2\alpha$ . Letting  $s = 1/2$  in  $\alpha = s/(s+1)$ , one gets  $\alpha = 1/3$ ,  $H = 1/3$ , and  $\beta = 2/3$ . Returning to Eq. (63), one infers  $\mu = 1$ . The latter exponent renders the limiting form (50) to the Riesz fractional operator in Eq. (49). Equation (50) tells us that the transport along the backbone is dominated by Cauchy-Lévy flights [81, 134], with the jump length distribution

$$\chi_\mu(\Delta x) \sim A_1(\Delta x)^{-2} \quad (64)$$

consistently with the probability density in Eq. (46). The asymptotic transport equation in the  $x$  direction is deduced from the general Eq. (57), where one employs  $\beta = 2/3$  and  $\mu \rightarrow 1$ . Using (50), one is led to a nonlocal (in the sense of the generalized central limit theorem [84, 85]) transport model

$$\frac{\partial}{\partial t} f(x, t) = -\frac{1}{\pi} {}_0D_t^{2/3} \left[ K_{2/3,1} \frac{\partial}{\partial x} \int_{-\infty}^{+\infty} \frac{f(x', t)}{x - x'} dx' \right]. \quad (65)$$

The nonlocal character of Eq. (65) is clear from the convolution operator on the right-hand side, which integrates the slowly decaying kernel  $\propto 1/(x - x')$  in infinite limits.

In fusion literature, there exists an impressive evidence that the spillover of turbulence into stable regions can be nonlocal, with a wealth of data involving edge turbulence [7, 42, 56, 60, 62], energetic particles [8, 105, 140, 141] and edge-SOL coupling [16–18, 22]. Our results indicate that nonlocal behavior is produced naturally through inelastic triad interactions in a multi-wave Hamiltonian system with the interaction Hamiltonian (6)—consistently with the fractional transport Eq. (65) and the Hilbert transform operator (51).

### B. Four-wave interactions

Mathematically, the four-wave interaction case is similar to triad interactions considered previously, yet it leads to a somewhat different kinetic description, as we now proceed to show.

Combining the scaling laws in Eqs. (22) and (63), one is led to  $\beta/\mu = 1/2$ . The distribution of waiting times is deduced from Eq. (35), where the  $\alpha$  value is obtained by letting  $s = 1$  in  $\alpha = s/(s+1)$ , from which  $\alpha = 1/2$ . Comparing to (56), one finds  $H = 1/2$  and  $\beta = 2H = 1$ . With the aid of Eq. (61) one gets  $1/\mu = 1/2$ , i.e.,  $\mu = 2$ . The transport model in Eq. (57) becomes

$$\frac{\partial}{\partial t} f(x, t) = {}_0D_t^{1/2} K_{1,2} \frac{\partial^2}{\partial x^2} f(x, t), \quad (66)$$

which contains the fractional derivative over time, but not over the space variable.

Note that the condition  $\mu = 2$  imposes a characteristic jump length in the  $x$  direction via a crossover to Gaussian statistics in the limit  $\mu \rightarrow 2$ . That means that the transport model in Eq. (66) satisfies the defining conditions of the central limit theorem [84, 86] and in this sense is local, in contrast to the nonlocal model in Eq. (65). This absence of nonlocal features is a distinct feature of four-wave interactions [67]. Yet, the model in Eq. (66) is non-Markovian (includes long-time correlations) owing to the Riemann-Liouville derivative  ${}_0D_t^{1/2}$  on the right-hand side.

The fundamental solution or Green's function of the time-fractional Eq. (66) can be expressed in terms of the Fox  $H$ -function (Appendix B of Ref. [79]) as

$$f(x, t) = \frac{1}{\sqrt{4\pi K_{1,2} t^{1/2}}} H_{1,2}^{2,0} \left[ \frac{x^2}{4K_{1,2} t^{1/2}} \middle| \begin{matrix} (3/4, 1/2) \\ (0, 1), (1/2, 1) \end{matrix} \right], \quad (67)$$

from which an asymptotic scaling  $\langle (\Delta x)^2(t) \rangle \propto t^{1/2}$  can be inferred for  $t \rightarrow +\infty$ .

It is understood that the subdiffusive transport scaling  $\langle (\Delta x)^2(t) \rangle \propto t^{1/2}$  occurs as a result of delta-coupling between the degrees of freedom in the original 2D Fokker-Planck model in Eq. (53). The effect this coupling has on asymptotic dynamics is that there is a waiting-time distribution between consecutive steps of the random walk along the  $x$  axis, motivating a reduced (fractional) model in Eq. (66). It is instructive to demonstrate how the original 2D model with coupling produces the same subdiffusive transport scaling  $\langle (\Delta x)^2(t) \rangle \propto t^{1/2}$  while containing all integer derivatives with respect to time  $t$  and also with respect to  $x$  and  $y$ . We have collected this demonstration in Appendix A.

### C. Special case

Turning to the zero-frequency resonance (i.e., the special case discussed in Sec. III), one combines the dispersion of a three-way interaction process, i.e.,  $\langle (\Delta n)^2(t) \rangle \propto t^{2/3}$ , with the distribution of waiting times dictated by four-wave interactions, i.e.,  $\chi_\alpha(\Delta t) \propto (\Delta t)^{-3/2}$ .

More explicitly, by matching the general dispersion law in Eq. (63) to the three-wave transport scaling in Eq. (41) one gets  $\beta/\mu = 2/3$ . On the other hand, by comparing the waiting-time distributions in Eqs. (42) and (56) one obtains  $H = 1/2$ ,  $\alpha = 1/2$  and  $\beta = 1$ , from which  $1/\mu = 2/3$  and  $\mu = 3/2$ . The distribution of the jump lengths in Eq. (46) becomes

$$\chi_\mu(\Delta x) \sim A_{3/2} |\Delta x|^{-5/2}, \quad (68)$$

where  $A_{3/2}$  is a normalization parameter. The resulting asymptotic transport equation is inferred from bi-fractional Eq. (57) by letting  $\beta = 1$  and  $\mu = 3/2$ , leading

to

$$\frac{\partial}{\partial t} f(x, t) = {}_0D_t^{1/2} K_{1,3/2} \frac{\partial^{3/2}}{\partial |x|^{3/2}} f(x, t). \quad (69)$$

This equation is different from Eq. (66) in that it contains the fractional derivatives with regard to *both* time  $t$  and the space variable  $x$  [similarly to Eq. (65) with Cauchy-Lévy flights].

### D. The $\mathbf{E} \times \mathbf{B}$ staircase as a Dirac comb

The mapping of the  $\mathbf{E} \times \mathbf{B}$  staircase (Sec. III) onto a Dirac comb is built in slab geometry as in Fig. 6. For symmetry reasons, the slab is drawn in proximity to the neutral line in the poloidal cross-section. The backbone coordinate  $x$  is in radial direction. The jet zonal flows are represented as teeth of the comb. The side coordinate  $y$  mimics the poloidal coordinate. We adopt a level of idealization according to which  $y$  is a Pythagorean coordinate, not a cyclic one. The cyclic case is mathematically similar, though is not considered here. Following Ref. [103], the period scale  $\Lambda$  between neighboring teeth is evaluated as the electrostatic Rhines length [142], i.e.,  $\Lambda \simeq \Lambda_{\text{Rh}}$ . Similarly to its celebrated fluid analog [122], the electrostatic Rhines length  $\Lambda_{\text{Rh}}$  designates the spatial scale separating vortex motion from drift wave-like motion. As such, it scales as the square root of the fluid (drift) velocity, i.e.,  $\Lambda_{\text{Rh}} \simeq \sqrt{|\mathbf{E} \times \mathbf{B}|}$ , where  $\mathbf{E}$  is the radial electric field, and  $\mathbf{B}$  is the toroidal magnetic field. Note that we employ a discrete comb as in Eq. (1), which is more suitable to represent the  $\mathbf{E} \times \mathbf{B}$  staircase, owing to a well-defined spacing between the jets, i.e.,  $\Lambda \simeq \Lambda_{\text{Rh}}$ .

A dynamical model is obtained by assuming that the random walker may occasionally jump (with the probability  $1/2$ , as it comes across the backbone) from the side branch on which it is currently sitting to another side branch: to either a neighboring one (a situation depicted in Fig. 6) or to a more distant one, with a Lévy distribution of the jump lengths as in Eq. (46). These model assumptions find support in the direct experimental observation of plasma avalanches [28, 127] and the fact that the staircase jets operate as semi-permeable [29, 30, 128] transport barriers to radial transport, i.e., whether or not an avalanche is absorbed by a given jet is probabilistic.

More so, the waiting-time distribution between consecutive jumps (consecutive emission-reabsorption events) is borrowed from Eq. (42) on account of the zero-frequency resonance (37), i.e.,  $\chi_\alpha(\Delta t) \propto (\Delta t)^{-3/2}$ . This last distribution, together with the distribution of the jump lengths in Eq. (68), leads directly to bi-fractional transport equation (69), where the fractional derivatives over time  $t$  and the spatial coordinate  $x$  incorporate the signatures of non-Markovianity and nonlocality, respectively.

One sees that the staircase dynamics is both long-time correlated ( $\alpha = 1/2$ ) and nonlocal ( $\mu = 3/2$ ).

It is understood that the Lévy distribution of the jump lengths in Eq. (46) implies a power-law distribution of

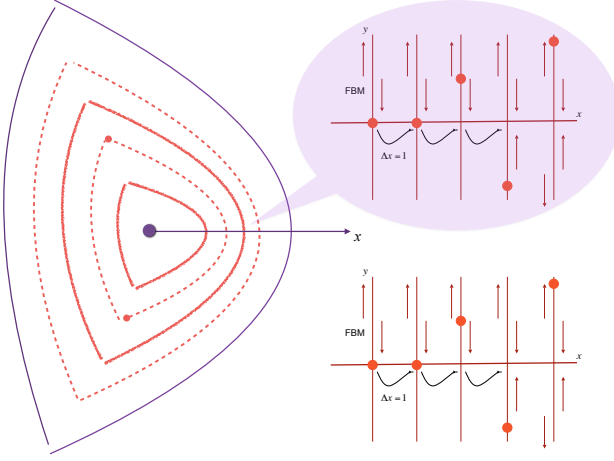


FIG. 6: The  $\mathbf{E} \times \mathbf{B}$  staircase as a Dirac comb. Left: a poloidal cross-section of magnetic flux surfaces in a tokamak. The flux surfaces are shown as alternating solid and dashed lines (red color). The plasma staircase occurs at a crossroads between the outer core and inner edge plasma and is enlarged at the top-right of the figure. The same structure is reproduced on the bottom-right. One associates the jet poloidal flows with side branches of the Dirac comb (see Fig. 1). The backbone direction, marked by the coordinate  $x$ , represents the radial direction in a tokamak. A test particle (random walker, red circle) can jump from the side branch on which it is currently sitting to either a neighboring branch (a situation shown in figure) or bypass the neighboring branch to land at a more distant location, such that there is a distribution of the jump lengths in accordance with the Lévy distribution in Eq. (46). Vertical arrows (both directions) represent the fractional Brownian motion (FBM) in side branches.

plasma avalanches over their sizes [103, 104], i.e.,

$$\chi_\mu(\ell) \sim A_\mu \ell^{-(1+\mu)}, \quad (70)$$

where by “size”  $\ell$  one means the radial distance traveled by an avalanche since its initial emission at one radial location and up to the absorption at another location some  $\ell$  radial steps away.

On the modeling side, the size distribution of plasma avalanches across the  $\mathbf{E} \times \mathbf{B}$  staircase has already been measured numerically in computer simulations [28–30] of the Tore Supra plasma using the GYSELA code [143]. The results from those simulations have been summarized [29, 30] in terms of a Fréchet distribution, which is a special case of Weibull (or generalized extreme value) distribution with lower bound [144]. For large avalanches for which  $\ell$  is in the order of the Rhines length or longer, i.e.,  $\ell \gtrsim \Lambda_{\text{Rh}}$ , a behavior compatible with the Pareto-Lévy distribution has been observed [104], i.e.,

$$\chi_\kappa(\ell) \sim A_\kappa \ell^{-(1+1/\kappa)}, \quad (71)$$

where  $\kappa$  is the fitting shape parameter, with the best fit found at  $\kappa \simeq 0.67$  (in the notation of Ref. [104],  $\ell \equiv \Delta n$  and  $\chi_\kappa \equiv \mathcal{F}_\kappa$ ). Comparing to Eq. (70), one identifies

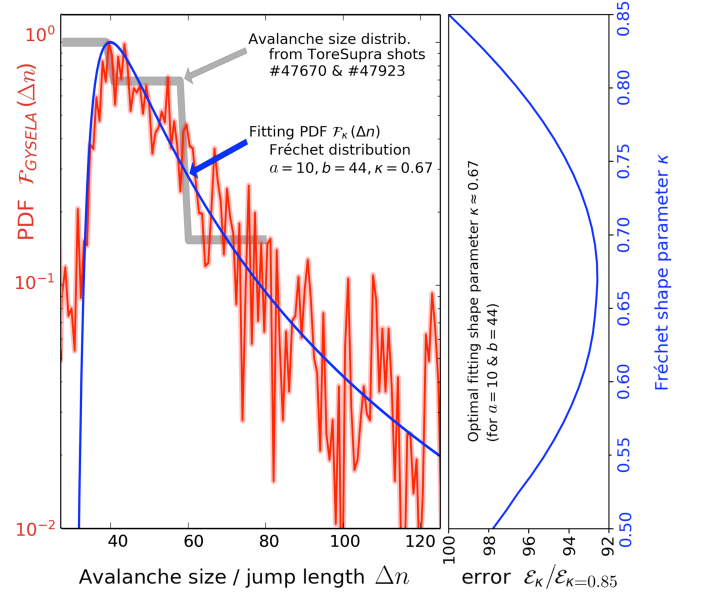


FIG. 7: The GYSELA computed probability density (red color) versus the Fréchet distribution with  $\kappa \simeq 0.67$  for which the optimum fit was obtained. Coarse experimental distribution is plotted in gray color. The right panel summarizes the normalized root-mean-square error in a percentile to the maximum error at  $\kappa \simeq 0.85$ , showing that the normalized error is minimized for  $\kappa \simeq 0.67$ . Adapted from Ref. [104].

the exponent  $1/\kappa$  with the Lévy index  $\mu$ , i.e.,  $\kappa = 1/\mu$ . Using  $\mu = 3/2$ , one infers  $\kappa = 2/3$ , which almost precisely reproduces the numerical result  $\kappa \simeq 0.67$ .

Here, for the reader’s convenience we incorporate a plot from Ref. [104], which reports the computed probability distribution  $\mathcal{F}_\kappa(\Delta n)$  versus the Tore Supra data and the approximations made. The plot, which is shown in Fig. 7, evidences on its right the optimal fitting shape parameter  $\kappa$ , with the extremum of fitting quality at  $\kappa \simeq 0.67$ . We interpret this close agreement with numerical simulations as an important milestone towards the validation of the comb model and the associated bi-fractional transport Eq. (69).

In the analysis of Ref. [104], a somewhat different estimate on the parameter  $\kappa$  was deduced theoretically, namely,  $\kappa = (\sqrt{17} + 1)/8 \simeq 0.64$ . This estimate is numerically close, though analytically not identical, to the value  $\kappa = 2/3$  predicted by the comb model. In particular, the value  $\kappa = 2/3$  is a rational number, while  $\kappa = (\sqrt{17} + 1)/8$  is an irrational one.

The discrepancy between the two values is not really surprising. In fact, the analysis of Ref. [104] builds upon a mean-field approximation [145] and uses as a basis the nonlinear Schrödinger equation with algebraic nonlinearity [113, 114]. On the contrary, the transport model in Eq. (69) assumes no reduction to mean-field dynamics as it refers directly to the three-wave interaction Hamiltonian in Eq. (6) (and the ensuing nonlocal character of field spreading). As a consequence, the comb model of



fers a more precise estimate on  $\kappa$  (or, at least, a better fit to simulations) by associating the turbulence spreading dynamics with backbone transport on the Dirac comb. The end result is  $\kappa = 1/\mu = 2/3$ .

## VII. FRACTIONAL RELAXATION EQUATION

Performing the Fourier transform of the bi-fractional Eq. (57) one obtains the fractional relaxation equation [79, 80]

$$\frac{d}{dt}\hat{f}(k, t) = -\tau_k^{-\beta/2} {}_0D_t^{1-\beta/2}\hat{f}(k, t), \quad (72)$$

where  $\hat{f}(k, t)$  denote the Fourier components of  $f(x, t)$  and we have introduced

$$\tau_k^{-\beta/2} = |k|^\mu K_{\beta, \mu}. \quad (73)$$

In writing Eq. (72) we took into account that the Fourier transform of the Riesz fractional derivative  $\partial^\mu/\partial|x|^\mu$  is  $-|k|^\mu$ , where one suppresses the imaginary unit  $i^\mu$  following a convention used in fractional calculus (Ref. [79], p. 26).

The solution of the fractional relaxation equation (72) satisfying the initial condition  $\hat{f}(k, t=0) = 1$  is given by the Mittag-Leffler function [79, 136, 146]

$$E_{\beta/2}[-(t/\tau_k)^{\beta/2}] = \sum_{m=0}^{\infty} \frac{[-(t/\tau_k)^{\beta/2}]^m}{\Gamma(1 + \beta m/2)}, \quad (74)$$

where  $\Gamma$  denotes the Euler gamma function. For  $t \gg \tau_k$ , the Mittag-Leffler function  $E_{\beta/2}[-(t/\tau_k)^{\beta/2}]$  is approximated by a power law

$$E_{\beta/2}[-(t/\tau_k)^{\beta/2}] \simeq \frac{1}{\Gamma(1 - \beta/2)} (t/\tau_k)^{-\beta/2}, \quad (75)$$

showing that  $\hat{f}(k, t) \simeq [(t/\tau_k)^{\beta/2}\Gamma(1 - \beta/2)]^{-1}$  for  $t \rightarrow +\infty$ . Assuming three-wave interactions ( $\beta = 2/3$ ) one has  $\hat{f}(k, t) \propto (t/\tau_k)^{-1/3}$ , while for four-wave interactions ( $\beta = 1$ ) one obtains  $\hat{f}(k, t) \propto (t/\tau_k)^{-1/2}$ .

These theory findings can be supported by experimental results from the CASTOR tokamak [147], according to which the relaxation function has a power-law shape  $\varphi_\alpha(\tau) \simeq (\tau/\tau_0)^{-\alpha}$ , with the  $\alpha$  value ranging between 0.3 and 0.5 depending on parameters of the plasma discharge and the time interval that is analyzed. We interpret this conformity to the CASTOR measurements as a confirmation that the relaxation dynamics is non-Markovian and involves a long-time power-law tail consistently with the Mittag-Leffler relaxation pattern in Eq. (75).

Another point of interest here is that the distribution of waiting times in Eq. (35) can be translated into a power-law frequency distribution in accordance with

$$\chi_\alpha(\omega) = \chi_\alpha(\Delta t) \frac{d}{d\omega} \Delta t \propto \omega^{1+\alpha} \omega^{-2} \simeq \omega^{-(1-\alpha)}. \quad (76)$$

More explicitly, we have  $\chi_\alpha(\omega) \propto \omega^{-2/3}$  for  $\alpha = 1/3$  and  $\chi_\alpha(\omega) \propto \omega^{-1/2}$  for  $\alpha = 1/2$ . Such frequency spectra have been observed in the edge region of different tokamaks [148–152] and discussed in terms of self-organized criticality [153–155].

## VIII. SUMMARY AND FINAL REMARKS

In summary, we have proposed a model of turbulence spreading driven by inelastic resonant interactions of waves on a lattice. The theory model, which we discuss, is inspired by the studies of quantum localization of dynamical chaos [68, 69, 72, 76, 112]. Yet so, it presents a few particularities, which may be seen in both the basic configuration, which we consider, and the mathematical formalism, which we apply.

In terms of configuration, we implement a setting according to which the noninteracting waves can propagate freely in a preferred direction, while being linearly localized in transverse direction. A situation of this kind is accounted in magnetically confined plasmas where, e.g., drift wave type waves propagate mainly in the poloidal direction perpendicular to the magnetic field and are excited by localized pressure gradients in the radial direction.

In terms of mathematical formalism, we deliberately avoided the introduction of the nonlinear Schrödinger equation as of Refs. [69, 72, 73, 76, 112]. Instead, we have based our analysis on the Hamiltonian of resonant wave-wave interaction and conservation laws. This way, we could pencil the similarities and differences between three- and four-wave interactions, while placing these interactions on essentially an equal footing.

In terms of asymptotic transport laws, we have seen that the asymptotic spreading is always *subdiffusive*, is faster with three-wave interactions, and is slower with four-wave interactions. The main difference is that three-wave interactions produce *nonlocal* dynamics with Lévy flights, while four-wave interactions do not do so. In the latter case, the dynamics is local, i.e., satisfies the defining conditions of the central limit theorem.

More explicitly, if the interactions are three-wave-like, then the asymptotic spreading is characterized universally by a subdiffusive transport scaling  $\Delta n \propto t^{1/3}$ . If four-wave-like, then by the scaling  $\Delta n \propto t^{1/4}$ . Scaling relationships of this form hold for the number of states (in our notation,  $\Delta n$ ). Yet so, one can translate these scalings into spatial (radial) spread with the aid of  $\Delta n \propto \Delta x$ , and by doing so pave the way to a comparison with known scalings from numerical simulations. In the case of three-wave interactions, our model predicts  $\Delta x \propto t^{1/3}$  in a remarkable coincidence with the F-KPP result [21].

From an energy-budget standpoint, three-wave triad interactions constitute a preferred transport channel as such interactions correspond to a lower-order correction to  $H_0$ , whereas four-wave interactions correspond to a higher-order correction. If both three- and four-wave in-

interactions are allowed by the dispersion relation, then the actual spreading is ruled by the three-wave nonlinear dynamics (because spreading is faster in that case).

A special case of the above theory is a situation when the interaction process involves the zero-frequency resonance between two high  $\mathbf{k}$  running waves and one low-frequency standing wave. We have seen this process corresponds to a very peculiar dynamical pattern, in which pattern the asymptotic dispersion is three-wave-like, while the distribution of waiting times is four-wave-like. We have associated this special case of mixed statistics with the self-organization of L-mode tokamak plasma into banded flows or staircases [27–30].

The various transport regimes studied in this paper's work (three-wave, four-wave, mixed) are collected for comparison in Table 1, where one also finds a summary of the exponents characterizing the corresponding 1D reduced transport models.

By examining Table 1 one sees that a common feature among all regimes is non-Markovianity, i.e., the nonlinear wave dynamics is long-time correlated in all cases. This is indeed characteristic and finds explanation [67, 114] in the simultaneous presence of domains of chaotic and regular motion, leading to some nonergodicity of asymptotic spreading [114]. In contrast, the nonlocal signatures are more restrictive in that they occur specifically by way of three-wave interactions or the zero-frequency resonance, but not really through four-wave interactions.

Further inspection of Table 1 suggests a set of unique signatures or fingerprints of three-wave interactions: a relatively fast asymptotic spreading complying with an  $\Delta x \propto t^{1/3}$  scaling; an explicitly nonlocal behavior with Cauchy-Lévy flights; and an algebraic, rather than exponential, tunneling pattern. The fingerprints of four-wave interactions are, on the contrary, a slower spreading conforming to an  $\Delta x \propto t^{1/4}$  behavior; the absence of flights; and an exponentially decaying density of the probability to spill over a barrier. Both spreading patterns appear to be non-Markovian, with a distribution of trapping times.

An important conclusion to be drawn from the above analysis is that both spreading and staircasing can be described based on the same mathematical formalism, using the Hamiltonian of inelastic wave-wave interaction and a mapping procedure into the comb space. From this perspective, one dares say *the plasma staircase is a very special case of turbulence spreading*, which is mediated by the zero-frequency resonance in Eq. (37). This observation explains the observed involvement [16, 17, 22] of turbulence spreading in the formation of staircase dynamical patterns and coupling to transport barriers.

From a kinetic viewpoint, we have seen that resonant wave-wave interactions, if three- or four-wave-like, induce a transport process of the CTRW type [82, 83, 85] and therefore lead to a theoretical description in terms of fractional-derivative equations [79–81]. In that regard, the comb approach is fundamental as it paves the way to obtain the fractional exponents of these equations *exactly* by mapping the lattice dynamics onto the Dirac comb.

Exponent	Three-wave	Four-wave	Staircase
$s$	1/2	1	Mixed <sup>a</sup>
$\alpha$	1/3	1/2	1/2
$H$	1/3	1/2	1/2
$\beta$	2/3	1	1
$\mu$	1	2	3/2
$\kappa$	1	N/A	2/3
Property	Three-wave	Four-wave	Staircase
$\langle(\Delta n)^2(t)\rangle$	$\propto t^{2/3}$	$\propto t^{1/2}$	$\propto t^{2/3}$
$\chi_\alpha(\Delta t)$	$\propto (\Delta t)^{-4/3}$	$\propto (\Delta t)^{-3/2}$	$\propto (\Delta t)^{-3/2}$
$\chi_H(\Delta t)$	$\propto (\Delta t)^{-4/3}$	$\propto (\Delta t)^{-3/2}$	$\propto (\Delta t)^{-3/2}$
$\chi_\mu( \Delta x )$	$\propto  \Delta x ^{-2}$	Gaussian	$\propto  \Delta x ^{-5/2}$
$\chi_\mu(\ell)^b$	$\propto \ell^{-2}$	N/A	$\propto \ell^{-5/2}$
$\chi_\alpha(\omega)$	$\propto \omega^{-2/3}$	$\propto \omega^{-1/2}$	$\propto \omega^{-1/2}$
$\hat{f}(k, t)$	$\propto (t/\tau_k)^{-1/3}$	$\propto (t/\tau_k)^{-1/2}$	$\propto (t/\tau_k)^{-1/2}$
Transport Eq.	Eq. (65)	Eq. (66)	Eq. (69)
Non-Markov	Yes, $\alpha = \frac{1}{3}$	Yes, $\alpha = \frac{1}{2}$	Yes, $\alpha = \frac{1}{2}$
Nonlocal	Yes, $\mu = 1$	No <sup>c</sup> , $\mu = 2$	Yes, $\mu = \frac{3}{2}$
Lévy flights	Yes <sup>d</sup> , $\mu = 1$	No <sup>e</sup> , $\mu = 2$	Yes, $\mu = \frac{3}{2}$

<sup>a</sup>The dispersion of asymptotic transport by plasma avalanches corresponds to three-wave interactions, with  $s = 1/2$ , while the distribution of waiting times is such as if the interactions are four-wave, with  $s = 1$ .

<sup>b</sup>If radial transport occurs in the form of avalanches.

<sup>c</sup>The general conditions of the central limit theorem apply [84, 85].

<sup>d</sup>Special value corresponding to Cauchy-Lévy flights [81, 134].

<sup>e</sup>Corresponds to the local limit of the Riesz fractional derivative and Gaussian distribution of the jump lengths [81, 134].

TABLE I: A summary of results and comparison between three- and four-wave interaction patterns. By examining the corresponding transport exponents one sees that spreading is faster in the case of three-wave interactions, in which case the asymptotic dynamics is nonlocal (involves Lévy flights). The special case of mixed statistics (i.e., the zero-frequency resonance) is reported separately under the heading Staircase. We associate this special case with the self-organization of L-mode tokamak plasma into banded flows or staircases. N/A means the quantity is not well-defined in the case of four-wave interactions.

Focusing on time-fractional Eq. (57), we have seen that the Riemann-Liouville derivative on the right-hand side of this equation stems from a reduction to 1D of a more general 2D Fokker-Planck equation with delta-coupling between the degrees of freedom. The observed connection between 1D equation with fractional differentiation over time and 2D Fokker-Planck equation with coupling sheds light on theoretical foundations of fractional kinetics [79, 80], an important topic in statistical physics of complex systems [81, 139].

By devising a comb approach to the staircase transport problem [28, 29] we inferred an estimate on the shape parameter  $\kappa$ , which characterizes the observed distributions [29, 30, 104] of plasma avalanches over their sizes (in terms of the Fréchet distribution). Our results indi-

cate that the  $\kappa$  value is given by the inverse Lévy index  $\mu$ , i.e.,  $\kappa = 1/\mu$ . Because, by its definition [79],  $\mu < 2$ , we have  $\kappa > 1/2$ , provided the statistical distributions are Lévy stable, as they should.

More so, we have discussed that the staircasing, i.e., the occurrence of quasiregular banded flows [27, 28] from a micro-turbulence background, is driven universally by the zero-frequency resonance in Eq. (37). In that regard, the interaction Hamiltonian (38) with intermediate coupled states predicts a nonlocal dynamics with the Lévy index  $\mu = 3/2$ , suggesting  $\kappa = 1/\mu = 2/3$ . This theoretical finding enabled by the comb approximation meets gracefully the numerical result  $\kappa \simeq 0.67$  [104] obtained from flux-driven gyrokinetics.

Overall, a subdiffusive spreading process with radial dispersion  $\langle(\Delta x)^2(t)\rangle \propto t^{2/3}$  sounds like an important lower bound on radial transport across the plasma staircase. We associate this lower bound with the effect of coupled transport barriers in vicinity of marginality.

Finally, we remark that the comb model proves to be an efficient and simple way to characterize the anisotropic transport processes in electrostatic drift-wave turbulence. Indirectly, it also characterizes the anisotropic particle dispersion in beta-plane turbulence due to the similarity between drift waves in plasmas and Rossby waves on the beta-plane [156]. In that respect, we note that such anisotropic transport has been studied numerically for electrostatic drift waves in Refs. [60–63] and for fluid turbulence in Refs. [157, 158].

### Acknowledgments

Helpful discussions with P. H. Diamond, G. Dif-Pradalier, X. Garbet and Y. Sarazin are acknowledged with thanks. A.V.M. would like to thank the Isaac Newton Institute for Mathematical Sciences, Cambridge, U.K., for support and hospitality during the programs “Anti-diffusive dynamics: from sub-cellular to astrophysical scales” and “Stochastic systems for anomalous diffusion,” where work on this paper was undertaken. This work was supported by EPSRC grants No. EP/R014604/1 and EP/Z000580/1. Partial support was received from a grant from the Simons Foundation.

### Appendix: The Fokker-Planck model with singular backbone term

Let us rewrite the Fokker-Planck equation (53) first in a more suitable for our analysis form

$$\frac{\partial}{\partial t} f(x, y, t) = \left[ \varrho \frac{\partial^2}{\partial y^2} + \delta(y) \frac{\partial^2}{\partial x^2} \right] f(x, y, t), \quad (\text{A.1})$$

where  $\varrho \propto K_1/K_2$  is the normalized coefficient of the transport process, and  $t$  is dimensionless time. Focusing on the backbone transport, because the Fokker-Planck

equation in Eq. (A.1) is symmetric with respect to the inversion  $x \rightarrow -x$ , it is convenient to set the coordinate  $x$  on the semi-axis  $0 \leq x < +\infty$ . This setting is technical and does not influence results. Concerning the coordinate  $y$ , we do not assume any restriction, thus letting  $-\infty < y < +\infty$ . As the random walk starts at the origin ( $x = 0, y = 0$ ), we may also impose

$$f(x = +\infty, y, t) = \partial_x f(x = +\infty, y, t) = 0, \quad (\text{A.2})$$

$$f(x, y = \pm\infty, t) = \partial_y f(x, y = \pm\infty) = 0, \quad (\text{A.3})$$

where  $\partial_x$  and  $\partial_y$  denote the partial derivatives along  $x$  and  $y$ , respectively. Concerning the boundary condition at  $x = 0$ , it is assumed that  $f(x = 0, y = 0, t) = C_0$ , where  $C_0 = \text{const}$  for all  $t > 0$ . The initial condition for  $t = 0$  is defined as  $f_0(x, y) \equiv f(x, y, t = 0) = C(x)\delta(y)$ , where  $C(x) = 0$  for  $x > 0$ .

The transport problem is solved straightforwardly by applying the Laplace transform with respect to time to both sides of the Fokker-Planck equation (A.1), yielding

$$s\hat{f}(x, y, s) = \left[ \varrho \frac{\partial^2}{\partial y^2} + \delta(y) \frac{\partial^2}{\partial x^2} \right] \hat{f}(x, y, s), \quad (\text{A.4})$$

where  $\hat{f}(x, y, s) = \hat{\mathcal{L}}[f(x, y, t)](s)$  is the Laplace image of  $f(x, y, t)$ . Equation (A.4) is supplied with the Laplace image of the boundary condition at  $x = 0$ , i.e.,

$$\hat{f}(x = 0, y = 0, s) = \int_0^{+\infty} e^{-st} f(x = 0, y = 0, t) dt, \quad (\text{A.5})$$

from which  $\hat{f}(x = 0, y = 0, s) = C_0/s$ . The solution to Eq. (A.4) is obtained using the Ansatz

$$\hat{f}(x, y, s) = e^{-|y|\sqrt{s/\varrho}} \phi(x, s), \quad (\text{A.6})$$

where  $\phi(x, s)$  has the sense of a probability distribution along the backbone in the Laplace space. Setting  $y = 0$  in Eq. (A.6), one infers  $\phi(x, s) = \hat{f}(x, y = 0, s)$ , where  $\hat{f}(x, y = 0, s) = \hat{\mathcal{L}}[f(x, y = 0, t)](s)$  is the Laplace image of  $f(x, y = 0, t)$ . Mathematically, it is convenient to introduce  $f_1(x, t) = \int_{-\infty}^{+\infty} f(x, y, t) dy$ , which integrates the probability density  $f(x, y, t)$  in side branches. In the Laplace domain, the function  $f_1(x, t)$  becomes

$$\hat{f}_1(x, s) = \hat{f}(x, y = 0, s) \int_{-\infty}^{+\infty} e^{-|y|\sqrt{s/\varrho}} dy, \quad (\text{A.7})$$

leading to

$$\hat{f}_1(x, s) = 2[\varrho/s]^{1/2} \phi(x, s), \quad (\text{A.8})$$

where Eq. (A.6) has been considered. Integrating both sides of Eq. (A.4) over  $y$  in infinite limits from  $-\infty$  to  $+\infty$ , and applying the boundary conditions in Eqs. (A.2) and (A.3), one gets

$$s\hat{f}_1(x, s) = \frac{\partial^2}{\partial x^2} \hat{f}(x, y = 0, s), \quad (\text{A.9})$$

from which, on account of Eq. (A.6),

$$s\hat{f}_1(x, s) = \frac{\partial^2}{\partial x^2}\phi(x, s) \quad (\text{A.10})$$

and

$$\phi(x=0, s) = \hat{f}(x=0, y=0, s) = \frac{C_0}{s}. \quad (\text{A.11})$$

Combining Eqs. (A.10) and (A.8), and solving the ensuing differential equation for  $\phi(x, s)$ , one gets, with the aid of Eq. (A.11),

$$\phi(x, s) = \frac{C_0}{s} \exp\left[-(4s\varrho)^{1/4}x\right]. \quad (\text{A.12})$$

The mean-squared displacement along the backbone is obtained by taking the second moment of the probability density function  $\phi(x, t)$ , i.e.,

$$\langle(\Delta x)^2(t)\rangle = \frac{1}{N(t)} \int_0^{+\infty} x^2 \phi(x, t) dx, \quad (\text{A.13})$$

where  $\phi(x, t) = \hat{\mathcal{L}}^{-1}\phi(x, s)$ ,  $\phi(x, s)$  is given by Eq. (A.12), and we have introduced

$$N(t) = \int_0^{+\infty} \phi(x, t) dx = \hat{\mathcal{L}}^{-1} \left[ \int_0^{+\infty} \phi(x, s) dx \right] \quad (\text{A.14})$$

to normalize  $\phi(x, t)$ . A simple calculation leads to

$$N(t) = C_0 \hat{\mathcal{L}}^{-1} \left[ \frac{1}{(4\varrho)^{1/4}} s^{-5/4} \right]. \quad (\text{A.15})$$

From Eq. (A.13) one also gets

$$\langle(\Delta x)^2(t)\rangle = \frac{1}{N(t)} \hat{\mathcal{L}}^{-1} \int_0^{+\infty} x^2 \phi(x, s) dx. \quad (\text{A.16})$$

Substituting  $\phi(x, s)$  from Eq. (A.12), and performing the improper integration over  $x$ , one obtains

$$\langle(\Delta x)^2(t)\rangle = 2C_0 \frac{1}{N(t)} \hat{\mathcal{L}}^{-1} \left[ \frac{1}{(4\varrho)^{3/4}} s^{-7/4} \right]. \quad (\text{A.17})$$

Calculating the inverse Laplace transform in Eqs. (A.15) and (A.17), one finds

$$N(t) \simeq (C_0/\sqrt{2})(t/\varrho)^{1/4}, \quad (\text{A.18})$$

$$\langle(\Delta x)^2(t)\rangle \simeq \frac{C_0/\sqrt{2}}{N(t)} (t/\varrho)^{3/4}, \quad (\text{A.19})$$

from which, combining Eqs. (A.18) and (A.19),

$$\langle(\Delta x)^2(t)\rangle \simeq A_\varrho (t/\varrho)^{1/2}, \quad (\text{A.20})$$

where  $A_\varrho$  is a numerical coefficient of the order of 1.

To reconstruct the full (two-dimensional) probability density in the comb space, i.e., the  $f = f(x, y, t)$  function, one needs to tame

$$f(x, y, t) = C_0 \mathcal{L}^{-1} \left[ \frac{1}{s} e^{-|y|\sqrt{s/\varrho}} e^{-x(4s\varrho)^{1/4}} \right] \quad (\text{A.21})$$

with the new normalization

$$N'(t) = C_0 \mathcal{L}^{-1} \left[ \frac{1}{s} \int_0^{+\infty} e^{-x(4s\varrho)^{1/4}} dx \int_{-\infty}^{+\infty} e^{-|y|\sqrt{s/\varrho}} dy \right]. \quad (\text{A.22})$$

Straightforward integration yields

$$N'(t) = \sqrt{2}C_0 \mathcal{L}^{-1} \left[ \varrho^{1/4} s^{-7/4} \right]. \quad (\text{A.23})$$

Upon Laplace inversion to the time domain,

$$N'(t) \simeq \sqrt{2}C_0 \varrho (t/\varrho)^{3/4}, \quad (\text{A.24})$$

where we omitted for simplicity a numerical coefficient due to the Euler gamma function. The mean-squared displacement in the  $x$  direction is written as the double integral

$$\langle(\Delta x)^2(t)\rangle = \frac{1}{N'(t)} \mathcal{L}^{-1} \left[ \int_0^{+\infty} \int_{-\infty}^{+\infty} x^2 \hat{f}(x, y, s) dx dy \right]. \quad (\text{A.25})$$

The expression in square brackets is expanded as

$$\left[ \dots \right] = \frac{C_0}{s} \int_0^{+\infty} x^2 e^{-x(4s\varrho)^{1/4}} dx \int_{-\infty}^{+\infty} e^{-|y|\sqrt{s/\varrho}} dy, \quad (\text{A.26})$$

where Eqs. (A.6) and (A.12) have been considered. Integrating over  $x$  and  $y$  in infinite limits, after a simple algebra one obtains

$$\langle(\Delta x)^2(t)\rangle = \sqrt{2}C_0 \frac{1}{N'(t)} \mathcal{L}^{-1} \left[ \varrho^{-1/4} s^{-9/4} \right]. \quad (\text{A.27})$$

Calculating the inverse Laplace transform, one gets

$$\langle(\Delta x)^2(t)\rangle \simeq \sqrt{2}C_0 \varrho \frac{1}{N'(t)} (t/\varrho)^{5/4}. \quad (\text{A.28})$$

Now substituting  $N'(t)$  from Eq. (A.24), one recovers the asymptotic scaling law

$$\langle(\Delta x)^2(t)\rangle \simeq A_\varrho (t/\varrho)^{1/2} \quad (\text{A.29})$$

consistently with Eq. (A.20).  $A_\varrho$  is obtained by keeping everywhere the coefficients dictated by Euler's integral and is left as an exercise to the reader.

One sees that the Fokker-Planck equation (A.1) leads to the same subdiffusive transport scaling  $\langle(\Delta x)^2(t)\rangle \propto t^{1/2}$  as the fractional kinetic Eq. (66) does. To this end, the use of fractional-derivative equations becomes a matter of taste: The reduction to 1D of the original 2D transport model (53) comes at a cost of introducing the Riemann-Liouville derivative (58) and accepting the formalism of the Fox  $H$ -function [see Eq. (67)].

- 
- [1] X. Garbet, L. Laurent, A. Samain, and J. Chinardet, *Nucl. Fusion* **34**, 963 (1994).
  - [2] L. Tao, M. R. E. Proctor, and N. O. Weiss, *Mon. Not. R. Astron. Soc.* **300**, 907 (1998).
  - [3] N. H. Brummell, T. L. Clune, and J. Toomre, *Astrophys. J.* **570**, 825 (2002).
  - [4] W. G. Large, J. C. McWilliams, and S. C. Doney, *Rev. Geophys.* **32**, 363 (1994).
  - [5] D. G. MacDonald and F. Chen, *J. Geophys. Res.* **117**, C05025 (2012).
  - [6] T. S. Hahm, P. H. Diamond, Z. Lin, K. Itoh, and S.-I. Itoh, *Plasma Phys. Control. Fusion* **46**, A323 (2004).
  - [7] V. Naulin, A. H. Nielsen, and J. Juul Rasmussen, *Phys. Plasmas* **12**, 122306 (2005).
  - [8] F. Zonca, S. Briguglio, L. Chen, G. Fogaccia, T. S. Hahm, A. V. Milovanov, and G. Vlad, *Plasma Phys. Control. Fusion* **48**, B15 (2006).
  - [9] Z. Lin and T. S. Hahm, *Phys. Plasmas* **11**, 1099 (2004).
  - [10] Ö. D. Gürcan, P. H. Diamond, T. S. Hahm and Z. Lin, *Phys. Plasmas* **12**, 032303 (2005).
  - [11] Ö. D. Gürcan, P. H. Diamond, and T. S. Hahm, *Phys. Plasmas* **13**, 052306 (2006).
  - [12] Ö. D. Gürcan and P. H. Diamond, *Phys. Plasmas* **14**, 055902 (2007).
  - [13] Z. B. Guo and P. H. Diamond, *Phys. Plasmas* **24**, 100705 (2017).
  - [14] P. Miglino, R. Buchholz, S. R. Grosshauser, W. A. Hornsby, A. G. Peeters, and O. Stauffert, *Nucl. Fusion* **56**, 014002 (2016).
  - [15] S. Yi, J. M. Kwon, P. H. Diamond, and T. S. Hahm, *Nucl. Fusion* **55**, 092002 (2015).
  - [16] T. S. Hahm and P. H. Diamond, *J. Kor. Phys. Soc.* **73**, 747 (2018).
  - [17] G. Dif-Pradalier, Ph. Ghendrih, Y. Sarazin, E. Caschera, F. Clairet, Y. Camenen, P. Donnel, X. Garbet, V. Grandgirard, Y. Munsch, L. Vermare, and F. Widmer, *Commun. Phys.* **5**, 229 (2022).
  - [18] R. Singh and P. H. Diamond, *Phys. Plasmas* **27**, 042308 (2020).
  - [19] M. Yagi, T. Ueda, S.-I. Itoh, M. Azumi, K. Itoh, P. H. Diamond, and T. S. Hahm, *Plasma Phys. Control. Fusion* **48**, A409 (2006).
  - [20] L. Schmitz, L. Zeng, T. L. Rhodes, J. C. Hillesheim, W. A. Peebles, R. J. Groebner, K. H. Burrell, G. R. McKee, Z. Yan, G. R. Tynan, P. H. Diamond, J. A. Boedo, E. J. Doyle, B. A. Grierson, C. Chrystal, M. E. Austin, W. M. Solomon, and G. Wang, *Plasma Phys. Control. Fusion* **54**, 073012 (2014).
  - [21] P. H. Diamond, S.-I. Itoh, K. Itoh, and T. S. Hahm, *Plasma Phys. Control. Fusion* **47**, R35 (2005).
  - [22] G. Dif-Pradalier, E. Caschera, Ph. Ghendrih, Y. Asahi, P. Donnel, X. Garbet, V. Grandgirard, G. Latu, C. Norscini, and Y. Sarazin, *Plasma and Fusion Research: Rapid Comm.* **12**, 1203012 (2017).
  - [23] P. A. Politzer, M. E. Austin, M. Gilmore, G. R. McKee, T. L. Rhodes, C. X. Yu, E. J. Doyle, T. E. Evans, and R. A. Moyere, *Phys. Plasmas* **9**, 1962 (2002).
  - [24] S. Tokunaga, H. Jhang, S. S. Kim, and P. H. Diamond, *Phys. Plasmas* **19**, 092303 (2012).
  - [25] B. Van Compernelle, G. J. Morales, J. E. Maggs, and R. D. Sydora, *Phys. Rev. E* **91**, 031102R (2015).
  - [26] R. A. Heinonen and P. H. Diamond, *Phys. Plasmas* **26**, 030701 (2019).
  - [27] G. Dif-Pradalier, P. H. Diamond, V. Grandgirard, Y. Sarazin, J. Abiteboul, X. Garbet, Ph. Ghendrih, A. Strugarek, S. Ku, and C. S. Chang, *Phys. Rev. E*, **82**, 025401(R) (2010).
  - [28] G. Dif-Pradalier, G. Hornung, Ph. Ghendrih, Y. Sarazin, F. Clairet, L. Vermare, P. H. Diamond, J. Abiteboul, T. Cartier-Michaud, C. Ehrlacher, D. Estève, X. Garbet, V. Grandgirard, Ö. D. Gürcan, P. Hennequin, Y. Kosuga, G. Latu, P. Maget, P. Morel, C. Norscini, R. Sabot, and A. Storelli, *Phys. Rev. Lett.* **114**, 085004 (2015).
  - [29] G. Dif-Pradalier, G. Hornung, X. Garbet, Ph. Ghendrih, V. Grandgirard, G. Latu, and Y. Sarazin, *Nucl. Fusion*, **57**, 066026 (2017).
  - [30] G. Hornung, G. Dif-Pradalier, F. Clairet, Y. Sarazin, R. Sabot, P. Hennequin, and G. Verdoolaege, *Nucl. Fusion*, **57**, 014006 (2017).
  - [31] X. Garbet, O. Panico, R. Varennes, C. Gillot, G. Dif-Pradalier, Y. Sarazin, V. Grandgirard, P. Ghendrih, and L. Vermare, *Phys. Plasmas* **28**, 042302 (2021).
  - [32] A. Ashourvan and P. H. Diamond, *Phys. Rev. E* **94**, 051202(R) (2016).
  - [33] A. Ashourvan, R. Nazikian, E. Belli, J. Candy, D. Eldon, B. A. Grierson, W. Guttenfelder, S. R. Haskey, C. Lasnier, G. R. McKee, and C. C. Petty, *Phys. Rev. Lett.* **123**, 115001 (2019).
  - [34] W. Liu, Y. Chen, R. Ke, G. McKee, Z. Yan, K. Fang, Z. Yang, Z. Gao, Y. Tan, and G. R. Tynan, *Phys. Plasmas* **28**, 012512 (2021).
  - [35] L. Qi, M. J. Choi, M. Leconte, T. S. Hahm, and J.-M. Kwon, *Nucl. Fusion*, **62**, 126025 (2022).
  - [36] B. Ph. van Milligen, I. Voldiner, B. A. Carreras, L. García, M. A. Ochando, and The TJ-II Team, *Nucl. Fusion* **63**, 016027 (2023).
  - [37] Z. Lin, S. Ethier, T. S. Hahm, and W. M. Tang, *Phys. Rev. Lett.* **88**, 195004 (2002).
  - [38] K. Ida, Z. Shi, H. J. Sun, S. Inagaki, K. Kamiya, J. E. Rice, N. Tamura, P. H. Diamond, G. Dif-Pradalier, X. L. Zou, K. Itoh, S. Sugita, Ö. D. Gürcan, T. Estrada, C. Hidalgo, T. S. Hahm, A. Field, X. T. Ding, Y. Sakamoto, S. Oldenburger, M. Yoshinuma, T. Kobayashi, M. Jiang, S. H. Hahn, Y. M. Jeon, S. H. Hong, Y. Kosuga, J. Dong, and S.-I. Itoh, *Nucl. Fusion* **55**, 013022 (2015).
  - [39] X. Chu, P. H. Diamond, and Z. Guo, *Nucl. Fusion* **62**, 066021 (2022).
  - [40] T. Wu, P. H. Diamond, L. Nie, M. Xu, Y. Yu, R. J. Hong, Y. H. Chen, J. Q. Xu, T. Long, Y. Zhang, Q. H. Yan, R. Ke, J. Cheng, W. Li, Z. H. Huang, L. W. Yan, X. Chu, Z. H. Wang, and C. Hidalgo, *Nucl. Fusion* **63**, 126001 (2023).
  - [41] D. del-Castillo-Negrete, P. Mantica, V. Naulin, J. Juul Rasmussen, and JET EFDA contributors, *Nucl. Fusion* **48**, 075009 (2008).
  - [42] F. Hariri, V. Naulin, J. Juul Rasmussen, G. S. Xu, and N. Yan, *Phys. Plasmas* **23**, 052512 (2016).
  - [43] J. E. Rice, C. Gao, M. L. Reinke, P. H. Diamond, N. T. Howard, H. J. Sun, I. Cziegler, A. E. Hubbard, Y.

- A. Podpaly, W. L. Rowan, J. L. Terry, M. A. Chilenski, L. Delgado-Aparicio, P. C. Ennever, D. Ernst, M. J. Greenwald, J. W. Hughes, Y. Ma, E. S. Marmar, M. Porkolab, A. E. White, and S. M. Wolfe, Nucl. Fusion **53**, 033004 (2013).
- [44] J. E. Rice, J. Citrin, N. M. Cao, P. H. Diamond, M. Greenwald, and B. A. Grierson, Nucl. Fusion **60**, 105001 (2020).
- [45] R. A. Fisher, Ann. Eugen. **7**, 355 (1937).
- [46] A. N. Kolmogorov, I. G. Petrovsky, and N. S. Piskunov, Bull. Univ. Moscow **1**(6), 1 (1937).
- [47] A. Kolmogoroff, I. Petrovsky, and N. Piscounoff, Clin. Cancer Res. **1**, 1 (1937).
- [48] P. H. Diamond and M. Malkov, Phys. Scr. **T98**, 63 (2002).
- [49] E.-J. Kim, P. H. Diamond, M. Malkov, T. S. Hahm, K. Itoh, S.-I. Itoh, S. Champeaux, I. Gruzinov, O. Gurcan, C. Holland, M. N. Rosenbluth, and A. Smolyakov, Nucl. Fusion **43**, 961 (2003).
- [50] Ö. D. Gürçan, P. H. Diamond, X. Garbet, V. Berionni, G. Dif-Pradalier, P. Hennequin, P. Morel, Y. Kosuga, and L. Vermare, Phys. Plasmas **20**, 022307 (2013).
- [51] Y. Kosuga, P. H. Diamond, G. Dif-Pradalier, and Ö. D. Gürçan, Phys. Plasmas **21**, 055701 (2014).
- [52] S. J. Zweben, J. A. Boedo, O. Grulke, C. Hidalgo, B. LaBombard, R. J. Maqueda, P. Scarin, and J. L. Terry, Plasma Phys. Control. Fusion **49**, S1 (2007).
- [53] P. Manz, T. T. Ribeiro, B. D. Scott, G. Birkenmeier, D. Carralero, G. Fuchert, S. H. Müller, H. W. Müller, U. Stroth, and E. Wolfrum, Phys. Plasmas **22**, 022308 (2015).
- [54] P. Manz, C. Hufnagel, A. Zito, D. Carralero, M. Griener, T. Lunt, O. Pan, M. Passoni, B. Tal, M. Wischmeier, E. Wolfrum, and ASDEX Upgrade Team, Phys. Plasmas **27**, 022506 (2020).
- [55] D.A. D'Ippolito, J.R. Myra, and S.J. Zweben, Phys. Plasmas **18**, 060501 (2011).
- [56] V. Naulin, J. Nucl. Materials **363-365**, 24 (2007).
- [57] A. Hasegawa and M. Wakatani, Phys. Rev. Lett. **50**, 682 (1983).
- [58] M. Wakatani and A. Hasegawa, Phys. Fluids **27**, 611 (1984).
- [59] W. Horton, Rev. Mod. Phys. **71**, 735 (1999).
- [60] V. Naulin, A. H. Nielsen, and J. Juul Rasmussen, Phys. Plasmas **6**, 4575 (1999).
- [61] V. Naulin, O. E. Garcia, A. H. Nielsen, J. Juul Rasmussen, Phys. Lett. A **321**, 355 (2004).
- [62] R. Basu, T. Jessen, V. Naulin, and J. Juul Rasmussen, Phys. Plasmas **10**, 2696 (2003).
- [63] R. Basu, V. Naulin, and J. Juul Rasmussen, Commun. Nonlinear Sci. Numer. Simul. **8**, 477 (2003).
- [64] A. V. Milovanov and J. Juul Rasmussen, Phys. Lett. A **378**, 1492 (2014).
- [65] G. M. Zaslavsky and R. Z. Sagdeev, *Introduction to the Nonlinear Physics. From Pendulum to Turbulence and Chaos* (Nauka, Moscow, 1988).
- [66] B. B. Kadomtsev, *Collective Phenomena in Plasmas* (Nauka, Moscow, 1988).
- [67] A. V. Milovanov, and J. Juul Rasmussen, Phys. Rev. E **109**, 045105 (2024).
- [68] D. L. Shepelyansky, Phys. Rev. Lett. **70**, 1787 (1993).
- [69] A. S. Pikovsky and D. L. Shepelyansky, Phys. Rev. Lett. **100**, 094101 (2008).
- [70] S. Flach, D. O. Krimer, and Ch. Skokos, Phys. Rev. Lett. **102**, 024101 (2009).
- [71] W.-M. Wang and Z. Zhang, J. Stat. Phys. **134**, 953 (2009).
- [72] Ch. Skokos, D. O. Krimer, S. Komineas, and S. Flach, Phys. Rev. E **79**, 056211 (2009).
- [73] Y. Krivolapov, S. Fishman, and A. Soffer, New J. Phys. **12**, 063035 (2010).
- [74] A. Iomin, Phys. Rev. E **81**, 017601 (2010).
- [75] B. Senyange, B. Many Manda, and Ch. Skokos, Phys. Rev. E **98**, 052229 (2018).
- [76] A. V. Milovanov and A. Iomin, Europhys. Lett. EPL **100**, 10006 (2012).
- [77] A. V. Milovanov and A. Iomin, Phys. Rev. E **89**, 062921 (2014).
- [78] I. Vakulchyk, M. V. Fistul, and S. Flach, Phys. Rev. Lett. **122**, 040501 (2019).
- [79] R. Metzler and J. Klafter, Phys. Rep. **339**, 1 (2000).
- [80] I. M. Sokolov, J. Klafter, and A. Blumen, Phys. Today **55**, 48 (2002).
- [81] R. Metzler and J. Klafter, J. Phys. A: Math. Gen. **37**, R161 (2004).
- [82] E. W. Montroll, and G. H. Weiss, J. Math. Phys. **6**, 167 (1965).
- [83] E. W. Montroll, and G. H. Weiss, J. Math. Phys. **10**, 753 (1969).
- [84] B. V. Gnedenko and A. N. Kolmogorov, *Limit Distributions for Sums of Independent Random Variables* (Addison-Wesley, Reading, 1954).
- [85] J.-P. Bouchaud and A. Georges, Phys. Rep. **195**, 127 (1990).
- [86] N. G. van Kampen, *Stochastic Processes in Physics and Chemistry* (North-Holland, Amsterdam, 1981).
- [87] J. A. Anta, J. Nelson, and N. Quirke, Phys. Rev. B **65**, 125324 (2002).
- [88] W. T. Coffey, J. Molecular Liquids **114**, 5 (2004).
- [89] A. V. Milovanov, K. Rypdal, and J. Juul Rasmussen, Phys. Rev. B **76**, 104201 (2007).
- [90] D. del-Castillo-Negrete, B. A. Carreras, and V. E. Lynch, Phys. Plasmas **11**, 3854 (2004).
- [91] B. Ph. van Milligen, R. Sánchez, and B. A. Carreras, Phys. Plasmas **11**, 2272 (2004).
- [92] D. del-Castillo-Negrete, Phys. Plasmas **13**, 082308 (2006).
- [93] B. A. Carreras, V. E. Lynch, B. Ph. van Milligen, and R. Sánchez, Phys. Plasmas **13**, 062301 (2006).
- [94] S. Havlin and D. ben-Avraham, Adv. Phys. **51**, 187 (2002); D. ben-Avraham and S. Havlin, *Diffusion and Reactions in Fractals and Disordered Systems* (Cambridge University Press, Cambridge, 2000).
- [95] S. R. White and M. Barma, J. Phys. A: Math. Gen. **17**, 2995 (1984).
- [96] Y. Gefen and I. Goldhirsch, J. Phys. A: Math. Gen. **18**, L1037 (1985).
- [97] G. H. Weiss and S. Havlin, Physica A **134**, 474 (1986).
- [98] T. A. L. Ziman, J. Phys. C: Solid State Phys. **12**, 2645 (1979).
- [99] P. G. de Gennes, La Recherche **7**, 919 (1976).
- [100] A. Iomin, V. Mèndez, and W. Horsthemke, *Fractional Dynamics in Comb-like Structures* (World Scientific, Singapore, 2018).
- [101] I. M. Sokolov, Soft Matter **8**, 9043 (2012).
- [102] A. Iomin, V. Zaburdaev, and T. Pfohl, Chaos, Solitons and Fractals **92**, 115 (2016).



- [103] A. V. Milovanov and J. Juul Rasmussen, Phys. Rev. E **98**, 022208 (2018).
- [104] A. V. Milovanov, J. Juul Rasmussen, and G. Dif-Pradalier, Phys. Rev. E **103**, 052218 (2021).
- [105] W. W. Heidbrink, Phys. Plasmas **15**, 055501 (2008).
- [106] D. J. Kaup, A. Reiman, and A. Bers, Rev. Mod. Phys. **51**, 275 (1979).
- [107] L. I. Schiff, *Quantum Mechanics* (McGraw Hill, New York, 1968).
- [108] G. P. Berman, A. M. Iomin, A. R. Kolovskii, and N. N. Tarhanov, *On the Dynamics of the Four-Wave Interactions in a Non-Linear Quantum Chain* (Kirenskii Physical Institute, Krasnoyarsk, 1986).
- [109] G. P. Berman and A. R. Kolovskii, Zh. Éksp. Teor. Fiz. **87**, 1938 (1984) [Sov. Phys. JETP **60** (6), 1116 (1984)].
- [110] G. M. Zaslavsky, *Statistical Irreversibility in Nonlinear Systems* (Nauka, Moscow, 1970).
- [111] M. V. Ivanchenko, T. V. Laptyeva, and S. Flach, Phys. Rev. B **89** 060301(R) (2014).
- [112] A. V. Milovanov and A. Iomin, Phys. Rev. E **95**, 042142 (2017).
- [113] A. V. Milovanov and A. Iomin, Phys. Rev. E **99**, 052223 (2019).
- [114] A. V. Milovanov and A. Iomin, Phys. Rev. E **107**, 034203 (2023).
- [115] J. E. Lennard-Jones, Proc. R. Soc. Lond. A **106** (738), 463 (1924).
- [116] G. M. Zaslavsky and B. V. Chirikov, Physics-Uspekhi **14**, 549 (1972).
- [117] B. V. Chirikov and V. V. Vecheslavov, Zh. Éksp. Teor. Fiz. **112**, 1132 (1997) [Sov. Phys. JETP **85** (3), 616 (1997)].
- [118] V. Rosenhaus and G. Falkovich, Phys. Rev. Lett. **133**, 244002 (2024).
- [119] J. Bardeen, L. N. Cooper, and J. R. Schrieffer, Phys. Rev. **108**, 1175 (1957).
- [120] L. Chen, Z. Lin, R. B. White, and F. Zonca, Nucl. Fusion **41**, 747 (2001).
- [121] K. Itoh, S.-I. Itoh, P. H. Diamond, T. S. Hahm, A. Fujisawa, G. R. Tynan, M. Yagi, and Y. Nagashima, Phys. Plasmas **13**, 055502 (2006).
- [122] D. G. Dritschel and M. E. McIntyre, J. Atmos. Sci. **65**, 855 (2008).
- [123] A. V. Milovanov, Phys. Rev. E **79**, 046403 (2009).
- [124] A. O. Korotkevich, A. I. Dyachenko, and V. E. Zakharov, Physica D **321-322**, 51 (2016).
- [125] T. Gheorghiu, F. Militello, and J. Juul Rasmussen, Phys. Plasmas **31**, 013901 (2024).
- [126] P. W. Terry, Rev. Mod. Phys. **72**, 109 (2000).
- [127] P. Beyer, S. Benkadda, X. Garbet, and P. H. Diamond, Phys. Rev. Lett. **85**, 4892 (2000).
- [128] A. Strugarek, Y. Sarazin, D. Zarzoso, J. Abiteboul, A. S. Brun, T. Cartier-Michaud, G. Dif-Pradalier, X. Garbet, Ph. Ghendrih, V. Grandgirard, G. Latu, C. Passeron, and O. Thomine, Phys. Rev. Lett. **111**, 145001 (2013).
- [129] W. B. Ewald, *From Kant to Hilbert: A Source Book in the Foundations of Mathematics, Volume 2* (Oxford University Press, Oxford, 2005).
- [130] R. R. Stoll, *Set Theory and Logic* (Dover Publications, San Francisco, CA, 1963).
- [131] B. B. Mandelbrot and J. Van Ness, SIAM Rev. **10**, 422 (1968).
- [132] B. B. Mandelbrot, *The Fractal Geometry of Nature* (W. H. Freeman, San Francisco, 1982).
- [133] J. Feder, *Fractals* (Plenum, New York, 1988).
- [134] R. Metzler, A. V. Chechkin, V. Yu. Gonchar, and J. Klafter, Chaos, Solitons and Fractals **34**, 129 (2007).
- [135] I. Podlubny, *Fractional Differential Equations* (Academic Press, San Diego, 1999).
- [136] S. G. Samko, A. A. Kilbas, and O.I. Marichev, *Fractional Integrals and Derivatives. Theory and Applications* (Gordon and Breach, Amsterdam, 1993).
- [137] F. Mainardi, Yu. Luchko, and G. Pagnini, Fract. Calc. Appl. Anal. **4**, 153 (2001).
- [138] V. E. Arkhincheev and E. M. Baskin, Sov. Phys. JETP **73**, 161 (1991).
- [139] A. Iomin and E. Baskin, Phys. Rev. E **71**, 061101 (2005).
- [140] F. Zonca, L. Chen, S. Briguglio, G. Fogaccia, A. V. Milovanov, Z. Qiu, G. Vlad, and X. Wang, Plasma Phys. Control. Fusion **57**, 014024 (2015).
- [141] L. Chen and F. Zonca, Rev. Mod. Phys. **88**, 015008 (2016).
- [142] V. Naulin, New J. Phys. **4**, 28.1 (2002).
- [143] Y. Sarazin, V. Grandgirard, J. Abiteboul, S. Allfrey, X. Garbet, Ph. Ghendrih, G. Latu, A. Strugarek, G. Dif-Pradalier, P. H. Diamond, S. Ku, C. S. Chang, B. F. McMillan, T. M. Tran, L. Villard, S. Jolliet, A. Bottino, and A. Angelino, Nucl. Fusion **51**, 103023 (2011).
- [144] L. de Haan and A. Ferreira, *Extreme Value Theory: An Introduction* (Springer, New York, 2007).
- [145] A. J. Leggett, Rev. Mod. Phys. **73**, 307 (2001).
- [146] R. Gorenflo, A. A. Kilbas, F. Mainardi, and S. V. Rogosin, *Mittag-Leffler Functions, Related Topics and Applications* (Springer Nature, Berlin, 2014).
- [147] E. Martines, M. Hron, and J. Stöckel, Plasma Phys. Control. Fusion **44**, 351 (2002).
- [148] P. H. Diamond and T. S. Hahm, Phys. Plasmas **2**, 3640 (1995).
- [149] R. Sanchez and D. Newman, Plasma Phys. Control. Fusion **57**, 123002 (2015).
- [150] B. A. Carreras, B. van Milligen, M. A. Pedrosa, R. Balbín, C. Hidalgo, D. E. Newman, E. Sánchez, M. Frances, I. García-Cortés, J. Bleuel, M. Endler, S. Davies, and G. F. Matthews, Phys. Rev. Lett. **80**, 4438 (1998).
- [151] M. A. Pedrosa, C. Hidalgo, B. A. Carreras, R. Balbín, I. García-Cortés, D. Newman, B. van Milligen, E. Sánchez, J. Bleuel, M. Endler, S. Davies, and G. F. Matthews, Phys. Rev. Lett. **82**, 3621 (1999).
- [152] T. L. Rhodes, R. A. Moyer, R. Groebner, E. J. Doyle, R. Lehmer, W. A. Peebles, and C. L. Rettig, Phys. Lett. A **253**, 181 (1999).
- [153] P. Bak, C. Tang, and K. Wiesenfeld, Phys. Rev. Lett. **59**, 381 (1987).
- [154] P. Bak, C. Tang, and K. Wiesenfeld, Phys. Rev. A **38**, 364 (1988).
- [155] H. J. Jensen, *Self-Organized Criticality. Emergent Complex Behavior in Physical and Biological Systems* (Cambridge University Press, Cambridge, 1998).
- [156] J. Pedlosky, *Geophysical Fluid Dynamics* (Springer, New York, 1987).
- [157] D. Elhmaïdi, A. Provenzale, and A. Babiano, J. Fluid Mech. **257**, 533 (1993).
- [158] A. Provenzale, Ann. Rev. Fluid Mech. **31**, 55 (1999).